JCI The Journal of Clinical Investigation

COP1-DET1-ETS axis regulates ERK transcriptome and sensitivity to MAPK inhibitors

Yuanyuan Xie, … , Ping Chi, Yu Chen

J Clin Invest. 2018. https://doi.org/10.1172/JCI94840.

Research Article In-Press Preview **Oncology** **Therapeutics**

Aberrant activation of MAPK signaling leads to activation of oncogenic transcriptomes. How MAPK signaling is coupled with transcriptional response in cancer is not fully understood. In gastrointestinal stromal tumor and melanoma, both with oncogenic MAPK activation, we find that ETV1 and other Pea3-ETS transcription factors are critical nuclear effectors of MAPK signaling that are regulated through protein stability. Expression of stabilized Pea3-ETS factors can partially rescue the MAPK transcriptome and cell viability after MAPK inhibition. To identify players involved in this process, we performed a pooled genome-wide RNAi screen using a novel fluorescence-based ETV1 protein stability sensor, and identified *COP1*, *DET1*, *DDB1*, *UBE3C*, *PSMD4*, and COP9 signalosome members. COP1 and DET1 loss led to decoupling between MAPK signaling and downstream transcriptional response, where MAPK inhibition failed to destabilize Pea3 factors and fully inhibit the MAPK transcriptome, thus resulting in decreased sensitivity to MAPK pathway inhibitors. We identified multiple COP1 and DET1 mutations in human tumors that were defective in degradation of Pea3-ETS factors. Two melanoma patients had de novo DET1 mutations arising after vemurafenib treatment. These observations indicate that MAPK signaling-dependent regulation of Pea3-ETS protein stability is a key signaling node in oncogenesis and therapeutic resistance to MAPK pathway inhibition.

COP1-DET1-ETS axis regulates ERK transcriptome and sensitivity to MAPK inhibitors

Yuanyuan Xie[1], Zhen Cao[1,2], Elissa W. P. Wong[1], Youxin Guan[1], Wenfu Ma[3], Jenny Q. Zhang[1], Edward G. Walczak[1], Devan Murphy[1], Leili Ran[1], Inna Sirota[1], Shangqian Wang[1], Shipra Shukla[1], Dong Gao[1], Simon R.V. Knott[4,5], Kenneth Chang[4], Justin Leu[1], John Wongvipat[1], Cristina R. Antonescu[6], Gregory Hannon[4,5,7], Ping Chi[1,2,8,*], Yu Chen[1,2,8,*]

[1]Human Oncology and Pathogenesis Program, Memorial Sloan Kettering Cancer Center, New York USA

[2]Weill Cornell Graduate School of Medical Sciences, Cornell University, New York, New York, USA.

[3]Structural Biology Program, Memorial Sloan Kettering Cancer Center, New York, USA

[4]Watson School of Biological Sciences, Cold Spring Harbor Laboratory, Cold Spring Harbor, New York, USA

[5]CRUK Cambridge Institute, University of Cambridge, Cambridge, UK

[6]Department of Pathology, Memorial Sloan Kettering Cancer Center, New York, USA

[7]Howard Hughes Medical Institute, Chevy Chase, Maryland, USA

[8]Department of Medicine, Memorial Sloan Kettering Cancer Center, New York. New York, USA.

***Correspondence:**

Ping Chi, MD, PhD

Memorial Sloan Kettering Cancer Center

1275 York Avenue

New York, NY 10065

Tel: 646-888-3338

e-mail: chip@mskcc.org

Yu Chen, MD, PhD

Memorial Sloan Kettering Cancer Center

1275 York Avenue

New York, NY 10065

Tel: 646-888-3356

e-mail: cheny1@mskcc.org

Authorship note: Y. Xie and Z. Cao contributed equally to this work

Conflict of interest: The authors have declared that no conflict of interest exists.

Abstract

Aberrant activation of MAPK signaling leads to activation of oncogenic transcriptomes. How MAPK signaling is coupled with transcriptional response in cancer is not fully understood. In two MAPK activated tumor types, gastrointestinal stromal tumor and melanoma, we find that ETV1 and other Pea3-ETS transcription factors are critical nuclear effectors of MAPK signaling that are regulated through protein stability. Expression of stabilized Pea3-ETS factors can partially rescue the MAPK transcriptome and cell viability after MAPK inhibition. To identify players involved in this process, we performed a pooled genome-wide RNAi screen using a novel fluorescence-based ETV1 protein stability sensor, and identified *COP1*, *DET1, DDB1*, *UBE3C, PSMD4* and COP9 signalosome members. COP1 or DET1 loss led to decoupling between MAPK signaling and downstream transcriptional response, where MAPK inhibition failed to destabilize Pea3 factors and fully inhibit the MAPK transcriptome, thus resulting in decreased sensitivity to MAPK pathway inhibitors. We identified multiple COP1 and DET1 mutations in human tumors that were defective in degradation of Pea3-ETS factors. Two melanoma patients had *de novo* DET1 mutations arising after vemurafenib treatment. These observations indicate that MAPK signaling-dependent regulation of Pea3-ETS protein stability is a key signaling node in oncogenesis and therapeutic resistance to MAPK pathway inhibition.

Introduction

The MAP kinase (MAPK/ERK) signaling pathway is aberrantly hyperactivated in multiple malignancies via prevalent mutations in *BRAF*, *NF1*, various Ras isoforms, *KIT* and other receptor tyrosine kinases. Molecular targeted therapies that inhibit hyperactive MAPK signalling in cancer, such as RAF and MEK inhibitors for $BRAF^{V600}$-mutant melanoma (1, 2) and KIT inhibitor therapy for *KIT/PDGFRA*-mutant gastrointestinal stromal tumor (GIST) (3, 4) have revolutionized cancer treatment. Yet, targeted therapies are hampered by heterogeneity in the depth and duration of response and eventual drug resistance. The mechanisms of resistance are heterogeneous. Approximately 50% of resistant cases harbor secondary genetic lesions that reactivate the MAPK pathway, such as mutations in *RAF, MEK, NF1*, *Ras* isoforms in melanoma and secondary *KIT* mutations in GIST (5-7). Additionally, adaptive and reversible alterations that alter gene expression have been shown to modulate therapeutic sensitivity without detectable genetic alterations (8, 9).

Physiologically, the MAPK signaling pathway couples extracellular signals to a multitude of intracellular responses, including critically transcriptional changes. Cancers with constitutively activated MAPK signaling exhibit elevated ERK-dependent transcriptional output and inhibition of this output is correlated with therapeutic response to targeted therapies (10, 11). While one characterized mode of transcriptional regulation is direct ERK-mediated phosphorylation of transcription factors (12-14), other mechanisms that dynamically couples ERK activity and modulates the nuclear transcriptional output response in ERK-dependent cancers has not been elucidated.

In GIST, the ETS factor, ETV1, is a lineage-specific master regulator that cooperates with *KIT/PDGFRA* activating mutations in pathogenesis (15-19). In cutaneous melanoma, ETV1

is recurrently amplified and cooperates with $BRAF^{V600E}$ activating mutation in oncogenesis (20, 21). The cooperative oncogenic effects of ETV1 with *KIT*- or *BRAF*- activating mutations is in part through ETV1 protein stabilization and MAPK pathway inhibition with either KIT or MEK inhibitors leads to rapid ETV1 degradation (15-17). This implicates the dynamic regulation of ETV1 protein stability as a critical mechanism to couple ERK activity to downstream nuclear transcriptional response in GIST and melanoma. Previously, COP1 has been shown to be an E3 ligase that mediated degradation of Pea3 transcription factors and in prostate cancer COP1 loss is an alternative mechanism to overexpress ETS factors to genomic translocation (22-25).

Here, we demonstrate that ETV1 and other Pea3 family members are critical downstream transcriptional mediators of MAPK signaling in GIST and melanoma. To identify genes involved in MAPK signaling-dependent regulation of ETV1 protein stability, we performed a pooled genome-wide shRNA screen using a fluorescently tagged ETV1 as high-throughput readout. We identified a set of genes including COP1, DET1, DDB1, and members of the COP9 signalosome, whose loss results in persistent stabilization of ETV1 protein levels despite MAPK pathway inhibition. We show that in addition to baseline stability, COP1 and DET1 regulate of MAPK signaling-dependent Pea3 family stability. COP1 and DET1 loss led to maintenance of ETV1 protein levels and maintenance of MAPK transcriptional output in the presence of MAPK/ERK pathway inhibitors, and result in therapeutic resistance *in vitro* and *in vivo*. We identified a number of COP1 and DET1 mutations in human cancers that are defective in Pea3 factor degradation. In particular, we found two melanoma patients with *de novo* DET1 mutations after vemurafenib resistance. These observations highlight that the MAPK signaling-Pea3 ETS protein stability axis is a central regulatory node that dynamically couples upstream signaling with nuclear transcriptional output in ERK-dependent cancer and shape the sensitivity to targeted

therapeutics. They also suggest that dysregulation of COP1, DET1 and likely other genes involved in the MAPK-dependent ETV1 protein stability regulation can converge on the same novel mechanism in mediating therapeutic resistance to MAPK pathway inhibition.

Results

Pea3 ETS factors are MAPK-nuclear effectors of MAPK signaling strength through direct regulation of negative-feedback regulators

Most GISTs harbor *KIT* mutations that activate multiple downstream signaling pathways including the MAPK, PI3K, and STAT3 pathways. To determine the contribution of downstream MAPK signaling to the mutant *KIT*-mediated transcriptional output, we compared the transcriptional changes of KIT and MAPK signaling perturbations by the KIT inhibitor imatinib and the MEK inhibitor PD325901 in three *KIT*-mutant GIST cell lines (GIST48, GIST882, and GIST-T1). In GIST48 cells that harbor a secondary imatinib resistance *KIT* mutation, PD325901caused greater ERK inhibition and ETV1 depletion than imatinib. In GIST882 cells, PD325901and imatinib were both durably potent. In GIST-T1 cells, imatinib caused durable MAPK pathway inhibition whereas PD325901 caused only transient inhibition with rapid rebound of ERK phosphorylation and stabilization of ETV1 proteins (Supplemental Figure 1A-C). Nevertheless, the transcriptome changes by imatinib and PD325901 were highly concordant in all three GIST cell lines. The magnitude of transcriptome change paralleled the effects on MAPK signaling inhibition, e.g. greater transcriptome changes with PD325901 than imatinib treatment in GIST48 cells, greater transcriptome changes with imatinib than PD325901 treatment in GIST-T1 cells, and similar transcriptome changes with imatinib and PD325901 treatment in GIST882 cells (Supplemental Figure 1D-F). This indicates that in GIST, the transcriptional output downstream of KIT mutation is primarily through MAPK.

To determine if ETV1 is a transcriptional effector of MAPK signaling in GIST and melanoma, we performed integrative analysis of the MAPK transcriptome, the ETV1 transcriptome, and the ETV1 cistrome in the three GIST cell lines and two *BRAF*^{V600E}-mutant

melanoma cell lines (A375 and Colo800). We generated the MAPK signaling-dependent transcriptome by profiling cells treated with the PD325901 in GIST48 and GIST882, imatinib in GIST-T1 (see Supplemental Figure 1D-F), and the RAF inhibitor, vemurafenib, in A375 and Colo800 (26). We next generated gene sets of ETV1-dependent genes by comparing cells infected with two independent ETV1-specific shRNA (ETV1sh1 and ETV1sh2) with scrambled control shRNA (shSCR) for all five cell lines. For GIST48, we added an additional gene set of siRNA-mediated *ETV1* knockdown as an orthogonal knockdown method. We supplemented these with custom gene sets of GIST-specific genes, mouse ICC-MY specific genes, and MAPK regulated genes (Supplemental Table 1).

We performed gene set enrichment analysis (GSEA) on the MAPK transcriptome for each cell line, employing our custom gene sets together with ~6,000 gene sets from the Molecular Signatures Database (MSigDB). The analysis showed that ETV1-regulated gene sets are significantly enriched among genes downregulated by MAPK pathway inhibition in both GIST and melanoma cells (Figure 1, Table 1, Supplemental Tables 2-6). The enrichment is higher within the same cell lineage than across different lineages, suggesting that MAPK signaling and ETV1 regulate both the lineage-specific transcriptome and a common transcriptome shared across different cell lineages. As expected, cell cycle gene sets and MAPK dependent gene sets were enriched in all cell lines. Since ETV1 is a GIST-lineage master regulator, GIST-lineage specific gene sets were highly enriched in GIST cell lines (Supplemental Tables 2-6).

We next performed ETV1 ChIP-seq in GIST-T1, A375, Colo800 cell lines and integrated with prior ETV1 ChIP-seq profiles in GIST48 and GIST882 cells (15, 19). We mapped global ETV1 peaks for each cell line, merged them and annotated them as promoter (TSS ± 1kb) and

enhancer peaks (non-promoter). ETV1 promoter binding was similar across all 5 cell lines (Figure 2A). ETV1 enhancer binding was far more divergent, consistent with known observation that enhancer localization is lineage-specific (19). We performed unsupervised k-means clustering of ETV1 enhancer peaks, which identified 3 clusters consisting of GIST-specific, melanoma-specific, and shared enhancer peaks (Figure 2A). Pairwise comparison confirmed higher concordance of peaks within each lineage than between the two lineages (Supplemental Figure 2). These data indicate that ETV1 binds to both common and lineage-specific sites.

We performed integrative analysis of the ETV1 cistrome with the MAPK regulated genes, defined in GIST as genes downregulated by PD325901 (GIST48, GIST882) or imatinib (GIST-T1) and in melanoma as genes downregulated by vemurafenib (A375, Colo800). We identified a common set of 17 genes that had ETV1 binding sites and were robustly regulated by MAPK signaling in both GIST and melanoma cells. Notably, within these genes are negative-feedback regulators of the RAS/MAPK pathway, including *DUSP6*, *SPRY2*, *SPRY4*, *SPRED1*, and *SPRED2* (Figure 2B-C). MAPK negative-feedback regulators are dynamically regulated in response to MAPK signaling activity and their expression levels are correlated with MAPK signaling output in cancer (10, 11). This observation suggests that ETV1 is involved in the homeostasis of MAPK signaling through direct regulation of the negative-feedback regulators.

To corroborate this, we performed siRNA mediated knockdown of ETV1 and its related Pea3 ETS factors (ETV4 and ETV5) due to their redundant function as ETV1, in GIST882 and A375 cells. Downregulation of individual and in particular all three Pea3 ETS factors decreased DUSP6 and SPRY4 levels. There was a paradoxical increase in upstream MAPK signaling evidenced by increased ERK phosphorylation, presumably due to de-repression of the negative-

feedback regulators (Figure 2D, Supplemental Figure 3). These data indicate that Pea3 ETS factors are MAPK signaling downstream effectors.

A genome-wide fluorescence-based MAPK-ETV1 protein stability sensor screen

We sought to identify factors that govern Pea3 ETS stability in response to MAPK signaling. In order to perform high-throughput whole genome screens for regulators of MAPK signaling-dependent ETV1 protein stability, we established a system to report ETV1 protein levels in individual living cells. We have chosen A2058 melanoma cells for the screen because 1) they harbor the *BRAF*^{V600E} mutation that constitutively activates the MAPK pathway to stabilize ETV1 protein, 2) the ETV1 protein levels can be dynamically destabilized by MAPK pathway inhibition by RAF or MEK inhibitors, and 3) they are resistant to growth suppression by MAPK pathway inhibition, which allows screening for ETV1 stability with MAPK inhibitor treatment without significant caveats of change in cell viability (27). We generated A2058 cells expressing MAPK-ETV1 stability sensors consisting of fusion proteins of ETV1 fragments with the green fluorescent EGFP and the red fluorescent tdTomato, under the same MSCV retroviral promoter with an internal ribosomal entry site (IRES) (Figure 3A) (28). We found that the amino-terminal 174 amino acids of ETV1, when fused to EGFP (EGFP-nETV1) was more robustly expressed than the full-length ETV1 (EGFP-flETV1) and maintained the MAPK signaling-dependent regulation of protein stability (Figure 3B). Because EGFP-nETV1 and tdTomato arise from the same transcript, the ratio of EGFP to tdTomato fluorescence in individual cells assayed by fluorescence-activated cell sorting (FACS) analysis is an indicator of EGFP-nETV1 protein stability. When the MAPK signaling was inhibited by either the RAF inhibitor, vemurafenib, or the *BRAF*-specific shRNA in A2058 cells, there was a robust decrease

in EGFP fluorescence with little change in tdTomato fluorescence, leading to a decrease in EGFP/tdTomato fluorescence ratio (Figure 3C-D).

To identify genes that regulate MAPK signaling-dependent ETV1 protein stability, we performed a pooled genome-wide RNAi screen using a mir-30 based shRNA library of ~76,000 hairpins targeting ~20,000 human genes (29, 30). To obtain hits that maintained ETV1 protein levels despite MAPK pathway inhibition, we treated the A2058 MAPK-ETV1 sensor cells with the vemurafenib for 24 hours prior to isolation of cells with highest and lowest 5% as well as the middle 20% of EGFP/tdTomato fluorescence ratio by FACS (Figure 3E). Sorted cells were cultured for 2 weeks and re-sorted twice, with 24 hours of vemurafenib treatment prior to each sort, for a total of three rounds to enrich hits. The shRNA-mir representation was determined at each sort by next-generation sequencing. We observed a progressive shift in hairpin representation in high and low EGFP/tdTomato-sorted cells compared to the middle EGFP/tdTomato-sorted cells, indicating that there was an enrichment of specific shRNAs in EGFP-high and EGFP-low populations (Supplemental Figure 4A). We used HiTSelect (31) to identify expressed genes whose hairpins are enriched in high EGFP/tdTomato-sorted cells (Table 2, Supplemental Figure 4B and Supplemental Tables 7-8). To decrease the number of off-target hits, we removed hits that were not expressed in A2058 cells (RPKM<1). The top hits, defined by genes ranked in the top 15 in sorts 2 or 3 and top 1000 in the other sort, included *COP1*, *DET1*, *DDB1* and multiple members of the COP9 signalosome (CSN). These belong to a group of genes termed constitutive photomorphogenic/de-etiolated/fusca (cop/det/fus) in plants (Figure 3F). Photomorphogenesis is a critical fate decision in plants; cop/det/fus genes couple light signals with transcriptionally regulated photomorphogenesis through regulating the protein stability of key transcription factors (32, 33). Mammalian COP1 and DET1 have been previously

identified to regulate protein degradation of Pea3 and other ETS factors at baseline (22, 24, 34). However, their roles in MAPK signaling-dependent regulation are not fully appreciated.

To validate the role of these candidates in MAPK signaling-dependent ETV1 protein stability regulation, we used the A375 melanoma cell line that harbors *BRAF*^{V600E} mutation and is sensitive to MAPK pathway inhibition. We engineered a mCherry-nETV1 protein stability sensor to simultaneously measure mCherry fluorescence to track ETV1 protein level and TurboGFP (tGFP) fluorescence to track shRNA-mir expression (Figure 3G-H). We used shRNAs with targeting sequences distinct from those in the screening library to target the top ranked candidate genes, including COP1, DET1, DDB1, a CSN member (COPS2), the ubiquitin receptor of the 26S proteosome PSMD4 and the ubiquitin ligase UBE3C. We transduced cells (MOI ~0.5) to express the shRNA only in a fraction of cells, which allows the non-transduced cells as internal controls for FACS analysis. The scrambled shRNA (SCR)-expressing tGFP-positive cells and the non-expressing tGFP-negative cells exhibited similar levels of baseline mCherry fluorescence with vehicle treatment, and mCherry fluorescence decrease with vemurafenib treatment. In contrast, tGFP-positive cells expressing shRNA against candidate genes exhibited increased baseline mCherry fluorescence with vehicle treatment, and diminished decrease of mCherry fluorescence upon vemurafenib treatment, indicating stabilized ETV1 protein (Figure 3H). These data indicate that COP1, DDB1, DET1 and the CSN are involved in MAPK-signaling dependent regulation of ETV1 protein stability.

COP1 couples MAPK signaling and Pea3 ETS-mediated transcriptome through dynamic protein stability regulation

To evaluate how MAPK signaling-dependent Pea3 ETS factor stability regulation influences the coupling of MAPK signaling-nuclear transcriptional output, we focused on COP1

which was previously shown to regulated Pea3 family ETS protein stability at baseline in prostate cancer (22, 23). In GIST (GIST882, GIST-T1) and melanoma (A375) cells, COP1 interacts with ETV1 endogenously (Supplemental Figure 5A). CRISPR/Cas9-mediated knockout of COP1 caused increased baseline protein levels of Pea3 ETS (ETV1, ETV4 and ETV5), and the MAPK negative-feedback regulators (e.g. DUSP6, SPRY4) with concomitant decrease in ERK phosphorylation (Supplemental Figure 5B). These data indicate that stabilized Pea3 ETS factors are sufficient to increase transcription of MAPK target genes.

We then examined the effect of COP1 depletion on MAPK regulated Pea3 ETS protein stability in GIST882 and A375 cells using siRNA-mediated knockdown of COP1 and CRISPR/Cas9 mediated knockout of COP1. In GIST882 cells treated with control siRNA (siSCR) or control guide RNA (sgCON), MAPK pathway inhibition by imatinib or PD325901 led to a rapid decrease in Pea3 ETS protein levels within 30 minutes. However, in GIST882 cells with RNAi or CRISPR/cas9-mediated downregulation of COP1 (siCOP1 or sgCOP1), Pea3 ETS protein levels were higher at baseline (vehicle), and maintained at high levels without any decrease despite MAPK pathway inhibition by imatinib or PD325901 (Figure 4A and Supplemental Figure 5C). Similarly, in A375 cells, COP1 depletion by siRNA or CRISPR/Cas9 increased baseline protein levels of Pea3 ETS and diminished the protein reduction in response to MAPK pathway inhibition by vemurafenib or trametinib (Figure 4B and Supplemental Figure 5D). In both cell lines, neither COP1 depletion nor MAPK pathway inhibitors significantly affected transcript levels of Pea3 ETS factors, indicating that the changes in protein levels were likely due to protein stability regulation (Supplemental Figure 6A-D).

Next, we examined the effect of COP1 loss on the global MAPK signaling-dependent transcriptome. We performed transcriptome analyses by RNA-seq in GIST882 cells transfected

with scrambled siRNA control (siSCR) or two independent COP1-specific siRNAs (COP1si), and then treated with vehicle or PD325901. To quantify a GIST882-specific MAPK-dependent transcriptome, we calculated a GIST882 MAPK score, which is the normalized median of genes downregulated by PD325901 treatment in siSCR-transfected GIST882 cells. The GIST882 MAPK score predictably decreased with PD325901 treatment and was not appreciably changed in the vehicle treatment group by COP1 knockdown. However, in PD325901 treated cells, COP1 knockdown cells exhibited significantly higher GIST882 MAPK score than siSCR control (Figure 5A). We performed this analysis using an independent MAPK signature (PRATILAS MAPK) (11) and obtained similar results (Supplemental Figure 7A). A heatmap of MAPK-regulated genes showed that COP1 knockdown in GIST cells treated with PD325901 reversed the transcriptome changes in response to PD325901 treatment or ETV1 knockdown alone (Figure 5B). We performed GSEA for gene sets that are enriched with PD325901 treatment in GIST882 cells and found a set of genes upregulated by COP1 knockdown in the presence of PD325901 is the most negatively enriched gene set (Figure 5C, Supplemental Table 3).

To extend these observations to melanoma, we calculated the A375 MAPK score, which is the normalized median of genes downregulated by vemurafenib treatment in siSCR-transfected A375 cells. As in GIST882 cells, COP1 loss partially restored MAPK transcriptional output after vemurafenib or trametinib treatment in A375 cells (Figure 5D-E, Supplemental Figure 7B). GSEA showed that a set of genes upregulated by COP1 knockdown in the presence of vemurafenib was the most enriched gene set among genes downregulated by vemurafenib (Figure 5F, Supplemental Table 5).

These data indicate that the coupling of MAPK signaling and downstream Pea3 ETS-mediated transcriptional response is mediated by dynamic signaling-dependent regulation of

protein stability; perturbation of this pathway by COP1 dysregulation can lead to decoupling of MAPK signaling and nuclear transcriptional output.

Decoupling of MAPK signaling and Pea3 ETS transcriptional response leads to resistance to MAPK targeted therapeutics

Reactivation of MAPK signaling through both genetic and non-genetic alterations represent a common pathway to resistance to MAPK pathway targeted therapies (6, 7, 9, 35). We next examined whether the decoupling of MAPK signaling and downstream transcriptional responses through COP1 loss can modulate sensitivity to MAPK pathway inhibition in GIST and melanoma.

In GIST-T1 cells, we employed competition proliferation assays between EGFP-positive CRISPR/Cas9-mediated COP1 knockout (sgCOP1) or EGFP-positive CRISPR/Cas9 empty-guide control cells (sgCON) with EGFP-negative uninfected cells treated with vehicle, imatinib, or trametinib (Figure 6A-B). In A375 cells, we employed competition proliferation assays in a mixed population of cells expressing shRNA-mir linked to tGFP (tGFP-positive) and control cells (tGFP-negative), and treated them with vehicle, vemurafenib, or trametinib (Figure 6D). For both cell types, COP1 loss (GFP-positive) cells enriched over time compared to the GFP-negative uninfected cells under the pressure of MAPK pathway inhibition, suggesting a growth advantage and fitness of the COP1 loss cells compared to COP1 intact controls under these conditions (Figure 6B, 6D). Additionally, we performed traditional drug treatment assays to determine the IC50 of imatinib and trametinib in GIST-T1 cells and IC50 of vemurafenib and trametinib in A375 cells with and without COP1 perturbation. We found a modest but consistent increase in IC50 in CRISPR/Cas9-mediated COP1 knockout cells compared to control cells (Figure 6C, 6E), indicating relative resistance to MAPK pathway inhibitor treatment. These data

indicate that COP1 is critical in modulating the MAPK signaling dependence of cancer cells and COP1 loss can lead to decreased sensitivity to therapies targeting the MAPK pathway in melanoma and GIST, presumably through protein stabilization of Pea3 ETS factors.

We next evaluated whether other hits in the COP1 degradation pathway from our screen (see Table 2) would exhibit similar behavior as COP1 when treated with MAPK pathway inhibitors. We performed growth competition assays using two independent shRNA against *DET1*, *DDB1*, *COPS2*, and *PSMD4* in A375 cells (Supplemental Figure 8A, B). *DET1* downregulation exhibited a similar growth advantage to COP1 loss, where the percentage of tGFP-positive cells remained stable with vehicle treatment, but increased significantly with vemurafenib or trametinib treatment. This data suggest that DET1 loss can mediate resistance to MAPK pathway inhibition. We found depletion of *DDB1*, *COPS2*, and *PSMD4* to be toxic and the percentage of tGFP-positive cells rapidly decreased with vehicle treatment. In the case of COPS2 and PSMD4, this growth decrease was partially rescued with MAPK pathway inhibition.

To corroborate that Pea3 ETS stability downstream of COP1 or DET1 loss mediates MAPK inhibitor resistance, we generated A375 cells with exogenous expression of wild-type ($ETV1^{WT}$) and a mutant ETV1 ($ETV1^{AAD}$) that has diminished binding to COP1 (22, 24) and therefore was resistant to COP1-mediated protein degradation in response to MAPK pathway inhibition by vemurafenib or trametinib (Figure 7A-C, Supplemental Figure 9). $ETV1^{WT}$ expression in A375 cells resulted in increased residual ETV1 protein after vemurafenib or trametinib treatment and caused modest resistance to MAPK pathway inhibition, consistent with previous observations (36) (Figure 7C-E). Moreover, the $ETV1^{AAD}$ protein is stable in response to vemurafenib and trametinib treatment in A375 cells (Figure 7C). $ETV1^{AAD}$ expression conferred increased resistance to MAPK pathway inhibition (Figures 7D-E). These data further

suggest that Pea3 ETS factor protein stabilization as a result of perturbation of the protein degradation pathway may reduce dependence on MAPK signaling and increase oncogenic fitness in response to MAPK pathway inhibition.

To determine if COP1 loss modulates sensitivity to MAPK pathway inhibition in GIST and melanoma *in vivo*, we treated GIST and melanoma xenografts with and without CRISPR/Cas9-mediated COP1 knockout. Short-term treatment of both GIST-T1 and A375 tumors recapitulated the *in vitro* observation and demonstrated that COP1 knockout xenografted tumors had increased baseline Pea3 ETS protein levels and diminished protein degradation in response to MAPK pathway inhibition (Figure 8A-B). In GIST-T1 xenografted tumors, COP1 knockout did not affect the *in vivo* growth when treated with vehicle, but exhibited diminished response to imatinib with development of early resistance compared to controls (Figure 8C). Similarly, COP1 knockout significantly diminished the growth suppressive effects by vemurafenib compared to controls in A375 xenografted tumors (Figure 8D). These data indicate that perturbation of the MAPK signaling-dependent Pea3 ETS protein stability regulatory axis can modulate sensitivity and lead to resistance to MAPK pathway inhibitors *in vivo*.

Characterization of COP1 and DET1 mutations in patient tumor samples

To study the clinical relevance of Pea3 ETS protein stability regulatory axis in MAPK-driven tumors, we examined the publically available oncogenomics data from a variety of patient cancer types via the MSK-cBioPortal (37). Since COP1 and DET1 loss were well tolerated at baseline and mediated MAPK-therapeutic resistance in preclinical models, we focused on identifying and characterizing the mutations of COP1 and DET1 in human cancers. In 23,083 tumors, COP1 (*RFWD2*) is homozygously deleted in 20 tumors (0.1%) and mutated in 191 (0.8%) including 37 truncating mutations. *DET1* is homozygously deleted in 5 tumors (0.02%)

and mutated in 117 (0.5%) including 16 truncating mutations. We next evaluated the functional consequences of the missense mutations in the functional domains of COP1 and DET1.

For COP1, there were two truncation mutations, E316* and E464*, both losing the substrate binding WD40 domain, and a number of missense mutations in melanoma. We engineered these missense mutations as well as several missense mutations in other cancer types that face the ligand binding pocket (Table 3) (38). To evaluate whether the point mutations affect the function of COP1, we generated CRISPR/Cas9-mediated COP1 knockout in A375 cells stably expressing mCherry-nETV1 protein stability sensor (see Supplemental Figure 5D). These sgCOP1 cells exhibited higher mCherry fluorescence at baseline which did not decrease upon vemurafenib treatment (Figure 9A-B). We next engineered COP1-IRES-EGFP with silent mutations at the sgCOP1 guide to resist editing and 14 missense mutations from melanoma and other cancers. We introduced these mutant COP1 proteins and used mCherry fluorescence to track ETV1 protein level and EGFP fluorescence to track COP1 mutant expression. We transduced cells at MOI ~50-60%, to express the COP1 mutants only in a fraction of cells, and the non-transduced cells served as internal controls for FACS analysis (Figure 9C-D). For EGFP-only control, EGFP positive cells exhibited similar mCherry fluorescence at baseline and after vemurafenib treatment. In contrast, for wild-type COP1, EGFP-positive cells exhibited decreased mCherry fluorescence that further decreased upon vemurafenib treatment. Cells expressing C159Y, W517C, C560R, W625S and G658E mutations had same levels of baseline mCherry fluorescence as EGFP-negative cells with or without MAPK inhibition, indicating they are non-functional. In addition, cells expressing R586C and N557S exhibited higher baseline mCherry fluorescence and attentuated fluorescence decrease with vemurafenib treatment, suggesting they are hypomorphic. The other mutations appear to be fully functional. Reference to the COP1 3D

crystal structure showed that most deleterious missense mutations localized near the binding surface on COP1 to ETV1 (Figure 9E). These data indicate that there are loss of function COP1 mutations in melanoma.

We next utilized a similar strategy to study DET1 mutations. Analysis of public datasets in cBioportal notably revealed that in a study of 32 paired pre-treatment and post-treatment of vemurafenib resistant samples, two samples showed *de novo* DET1 mutations after treatment (Table 4) (6). One of the two mutations, P535F, was also seen in a TCGA cutaneous melanoma sample (TCGA-FS-A4FB-06). We thus focused on these two missense mutations. We generated DET1 knockout A375 cells expressing mCherry-nETV1 protein stability sensor. Similar to COP1 knockout cells, DET1 knockout cells had higher levels of Pea3 factors at baseline that did not decrease after MAPK inhibition (Figure 10A). They also exhibited higher mCherry-nETV1 fluorescence at baseline that did not decrease upon vemurafenib treatment (Figure 10B-C). We expressed DET1-IRES-EGFP with silent mutations to escape sgDET1 CRISPR editing. Compared to wild-type DET1, DET1-P535F was completely defective in mCherry-nETV1 degradation and DET1-A429G exhibited attenuated activity (Figure 10D-E). These data suggests that mutations in COP1/DET1 may mediate MAPK inhibitor resistance in the clinic.

Discussion

The MAPK/ERK pathway is a central signaling pathway for many cellular processes, including proliferation, differentiation, and survival. With physiologic signaling, the transcriptional response is coupled to MAPK pathway activation, which is intricately regulated and depends on both the type and duration of upstream stimulus. Negative-feedback regulators of the MAPK pathway, such as the ERK phosphatase DUSP6, are strongly induced to limit the intensity and duration of ERK pathway activation, and maintain homeostasis of MAPK signaling (11). In cancer, tumors harboring constitutive MAPK/ERK activation express high levels of negative-feedback regulators that are often used as a surrogate biomarker for MAPK/ERK pathway signaling strength, and their rapid decline upon MAPK pathway inhibition indicates therapeutic efficacy, but is also exploited by cancer cells for early adaptation, development of persistent disease and eventual emergence of resistant disease (11, 39).

The development of potent inhibitors of the MAPK/ERK pathway has revolutionized cancer treatment. Yet, treatment response is rarely complete or durable and resistance invariably emerges. The mechanisms of secondary resistance have been extensively studied. Exome sequencing studies have shown that ~50% of resistant tumors harbor secondary mutations that reactivate the MAPK/ERK pathway (5, 40). Non-mutational mechanisms that govern drug sensitivity are not fully understood and can involve reversible cell autonomous or micro-environment mediated tuning of the MAPK/ERK pathway activity (8, 9, 41-43). The strength of coupling between upstream MAPK/ERK signaling with downstream transcriptional response can modulate MAPK inhibitor response as failure to turn off transcription in response to MAPK inhibition may increase drug tolerance.

Here, we have uncovered a novel mechanism that couples the upstream MAPK-signaling and downstream transcriptional output via COP1/DET1/CSN mediated signaling-dependent regulation of Pea3 ETS protein stability. Disruption of Pea3 ETS degradation through COP1 or DET1 loss results in decoupling of MAPK/ERK signaling and MAPK/ERK transcriptional output, where increased protein levels of Pea3 ETS factors results in increased levels of ERK feedback regulators regardless of ERK phosphorylation levels. In response to MAPK inhibition, COP1 loss cells can sustain MAPK dependent transcriptional output, resulting in increased cell viability and oncogenic fitness. Thus, MAPK/ERK-dependent transcriptional output and intact coupling is critical to MAPK inhibitor response, and the ERK phosphorylation level is only reliable when the coupling of the MAPK signaling-transcriptional response is intact. Moreover, perturbation of the axis of MAPK signaling-Pea3 ETS stability-transcriptional output can alter the sensitivity and potentially led to therapeutic resistance to MAPK pathway inhibitors in vitro and in vivo.

We have analyzed a study of 32-paired samples of pretreatment and post-resistance melanoma samples and identified two patients with de novo deleterious DET1 mutations in the post treatment sample, suggesting that mutations in DET1 are clinically relevant. The prevalence of alterations in the COP1/DET1/CSN pathway in mediating clinical resistance is not known due to the limited number of samples at this time and the large number of players in this pathway. In addition, two recent publications showed that loss of the tumors suppressor CIC, a well-known transcriptional suppressor of Pea3 ETS factors, conveyed resistance to MEK inhibition in pancreatic cancer (44) and EGFR inhibition in NSCLC (45). These studies highlight the multiple mechanisms to modulate Pea3 ETS factor levels in shaping response to MAPK inhibition.

Signal mediated regulation of transcription (co-)factor protein degradation is a mechanism in several crucial signaling pathways, including WNT signaling to β-catenin/TCF, DNA damage signaling to P53, and hypoxia signaling to HIF. Our work highlights the importance of dynamically regulated Pea3 factor protein stability in signaling-dependent transcription output of the MAPK pathway in oncogenic transformation and underline a novel mechanism of MAPK targeted therapeutic resistance.

Methods

Detailed methods are described in the Supplemental Methods.

In vivo tumorigenicity and drug treatment assays

For xenograft studies, 5×10^6 GIST-T1 cells and 1×10^6 A375 cells resuspended in 100 µL of 1:1 mix of growth media and Matrigel (#356237, BD Biosciences) were subcutaneously injected into CB17-SCID mice (#CB17SC-F, Taconic). Tumors were allowed to establish growth (6 weeks for GIST-T1 and 12 days for A375) after implantation before initiation of treatment. Mice were treated twice daily with MAPK pathway inhibitors or vehicle via orally gavage. Tumor sizes were measured twice a week with callipers, and were calculated using the following formula: tumor volume = $(D \times d^2)/2$, whereby D and d refer to the long and short tumor diameter, respectively. For short-term treatment, xenografts were explanted after 2 days of drug treatment. To generate lysates for Western blotting, tissue was homologized in SDS lysis buffer 1%SDS, 20mM NaF, 5mM EDTA and proteinase/phosphatase inhibitors using the FastPrep-24 system with Lysing Matrix A (MP Biomedicals). For long-term treatment, xenografts were treated twice daily until the end of the experiments.

Statistics

All statistical comparisons between two groups were performed by GraphPad Prism software 6.0 using a two-tailed unpaired t-test. The variance between the statistically compared groups was similar. A P value less than 0.005 was considered significant.

Study approval

All animal experiments were performed in accordance with a protocol reviewed and

approved by Memorial Sloan-Kettering Cancer Center Institutional Animal Care and Use Committee (#11-12-029) (New York, New York, USA).

Author Contribution

Experimental design: Y. X., Z.C., C.L.S., P.C. and Y.C.; shRNA screen: Z.C., Y.X., Q.Z., Y.G., S.R.V.K., K.C., G.H., C.L.S.; RNAi: Y.X., I.S.; Western blots: Y.X. and Z.C.; Immunoprecipitation: Y.X.; ChIP, ChIP-seq and RNA-seq: P.C., Y.C., Y.X., I.S. and E.W.P.W.; Generation of the expression vectors: Y.X., Z.C., Y.G. and J. L.; mCherry nETV1 protein stability assay: Y.X. and Y.G.; Xenograft: Y.X., D.M., E.G.W., L.R. and J.W.; Growth Competition Assay and FACS: Y.X., Q.Z., Z.C.; CRISPR/Cas9-Mediated Knockout: Y.X. and Z.C.; Structure modeling: W. M.; Manuscript writing: Y.X., Z.C., Y.C. and P.C.. All authors reviewed and edited the manuscript

Acknowledgements

We like to thank Corynn Kasap, Mary Klein, Terri McBride (Bella) and Karey Zheng for reagent development, Drs. Solit, Fletcher, Massagué and Taguchi for cell lines, Drs. Sawyers, Fagin and Rosen for critical review of the manuscript. Next generation sequencing and gene expression arrays were done at the Memorial Sloan Kettering Cancer Center (MSKCC) Genomics Core Facility. FACS sorting was performed at the MSKCC Flow Cytometry Core. This work was supported by grants from the NCI (K08CA140946 YC; R01CA193837 , YC; P50CA092629, YC; P50CA140146, PC, CRA; K08CA151660, PC; DP2 CA174499, PC), US DOD (W81XWH-10-1-0197), Prostate Cancer Foundation (YC), Starr Cancer Consortium (YC, PC), Geoffrey Beene Cancer Research Center (YC, PC), Gerstner Family Foundation (YC), Bressler Scholars Fund (YC), GIST Cancer Research Fund (PC, CRA), Shuman Fund (PC, CRA) and GIST Cancer Awareness Fund (PC).

References

1. Chapman PB, et al. Improved survival with vemurafenib in melanoma with BRAF V600E mutation. *N Engl J Med.* 2011;364(26):2507-16.
2. Flaherty KT, et al. Improved survival with MEK inhibition in BRAF-mutated melanoma. *N Engl J Med.* 2012;367(2):107-14.
3. Corless CL, et al. PDGFRA mutations in gastrointestinal stromal tumors: frequency, spectrum and in vitro sensitivity to imatinib. *J Clin Oncol.* 2005;23(23):5357-64.
4. Demetri GD, et al. Efficacy and safety of imatinib mesylate in advanced gastrointestinal stromal tumors. *N Engl J Med.* 2002;347(7):472-80.
5. Shi H, et al. Acquired resistance and clonal evolution in melanoma during BRAF inhibitor therapy. *Cancer Discov.* 2014;4(1):80-93.
6. Van Allen EM, et al. The genetic landscape of clinical resistance to RAF inhibition in metastatic melanoma. *Cancer Discov.* 2014;4(1):94-109.
7. Poulikakos PI, et al. RAF inhibitor resistance is mediated by dimerization of aberrantly spliced BRAF(V600E). *Nature.* 2011;480(7377):387-90.
8. Das Thakur M, et al. Modelling vemurafenib resistance in melanoma reveals a strategy to forestall drug resistance. *Nature.* 2013;494(7436):251-5.
9. Sun C, et al. Reversible and adaptive resistance to BRAF(V600E) inhibition in melanoma. *Nature.* 2014;508(7494):118-22.
10. Dry JR, et al. Transcriptional pathway signatures predict MEK addiction and response to selumetinib (AZD6244). *Cancer Res.* 2010;70(6):2264-73.
11. Pratilas CA, et al. (V600E)BRAF is associated with disabled feedback inhibition of RAF-MEK signaling and elevated transcriptional output of the pathway. *Proc Natl Acad Sci U S A.* 2009;106(11):4519-24.
12. Marais R, Wynne J, and Treisman R. The SRF accessory protein Elk-1 contains a growth factor-regulated transcriptional activation domain. *Cell.* 1993;73(2):381-93.
13. Slack C, Alic N, Foley A, Cabecinha M, Hoddinott MP, and Partridge L. The Ras-Erk-ETS-Signaling Pathway Is a Drug Target for Longevity. *Cell.* 2015;162(1):72-83.
14. Wasylyk B, Hagman J, and Gutierrez-Hartmann A. Ets transcription factors: nuclear effectors of the Ras-MAP-kinase signaling pathway. *Trends Biochem Sci.* 1998;23(6):213-6.
15. Chi P, et al. ETV1 is a lineage survival factor that cooperates with KIT in gastrointestinal stromal tumours. *Nature.* 2010;467(7317):849-53.
16. Hayashi Y, et al. Platelet-Derived Growth Factor Receptor-alpha Regulates Proliferation of Gastrointestinal Stromal Tumor Cells With Mutations in KIT by Stabilizing ETV1. *Gastroenterology.* 2015;149(2):420-32 e16.
17. Ran L, et al. Combined inhibition of MAP kinase and KIT signaling synergistically destabilizes ETV1 and suppresses GIST tumor growth. *Cancer Discov.* 2015;5(3):304-15.
18. Ran L, et al. ETV1-Positive Cells Give Rise to BRAFV600E -Mutant Gastrointestinal Stromal Tumors. *Cancer Res.* 2017;77(14):3758-65.
19. Ran L, et al. FOXF1 defines the core-regulatory circuitry in gastrointestinal stromal tumor (GIST). *Cancer Discov.* 2017.
20. Jane-Valbuena J, et al. An oncogenic role for ETV1 in melanoma. *Cancer Res.* 2010;70(5):2075-84.

21. Mehra R, et al. Comprehensive Analysis of ETS Family Members in Melanoma by Fluorescence In Situ Hybridization Reveals Recurrent ETV1 Amplification. *Transl Oncol.* 2013;6(4):405-12.
22. Vitari AC, et al. COP1 is a tumour suppressor that causes degradation of ETS transcription factors. *Nature.* 2011;474(7351):403-6.
23. Migliorini D, et al. Cop1 constitutively regulates c-Jun protein stability and functions as a tumor suppressor in mice. *J Clin Invest.* 2011;121(4):1329-43.
24. Baert JL, Monte D, Verreman K, Degerny C, Coutte L, and de Launoit Y. The E3 ubiquitin ligase complex component COP1 regulates PEA3 group member stability and transcriptional activity. *Oncogene.* 2010;29(12):1810-20.
25. Chen Y, et al. ETS factors reprogram the androgen receptor cistrome and prime prostate tumorigenesis in response to PTEN loss. *Nat Med.* 2013;19(8):1023-9.
26. Obenauf AC, et al. Therapy-induced tumour secretomes promote resistance and tumour progression. *Nature.* 2015;520(7547):368-72.
27. Xing F, et al. Concurrent loss of the PTEN and RB1 tumor suppressors attenuates RAF dependence in melanomas harboring (V600E)BRAF. *Oncogene.* 2011.
28. Yen HC, Xu Q, Chou DM, Zhao Z, and Elledge SJ. Global protein stability profiling in mammalian cells. *Science.* 2008;322(5903):918-23.
29. Knott SR, et al. A computational algorithm to predict shRNA potency. *Mol Cell.* 2014;56(6):796-807.
30. Bose R, et al. ERF mutations reveal a balance of ETS factors controlling prostate oncogenesis. *Nature.* 2017.
31. Diaz AA, Qin H, Ramalho-Santos M, and Song JS. HiTSelect: a comprehensive tool for high-complexity-pooled screen analysis. *Nucleic Acids Res.* 2015;43(3):e16.
32. Schwechheimer C, and Deng XW. The COP/DET/FUS proteins-regulators of eukaryotic growth and development. *Semin Cell Dev Biol.* 2000;11(6):495-503.
33. Lau OS, and Deng XW. The photomorphogenic repressors COP1 and DET1: 20 years later. *Trends Plant Sci.* 2012;17(10):584-93.
34. Lu G, et al. Phosphorylation of ETS1 by Src family kinases prevents its recognition by the COP1 tumor suppressor. *Cancer Cell.* 2014;26(2):222-34.
35. Wilson TR, et al. Widespread potential for growth-factor-driven resistance to anticancer kinase inhibitors. *Nature.* 2012;487(7408):505-9.
36. Johannessen CM, et al. A melanocyte lineage program confers resistance to MAP kinase pathway inhibition. *Nature.* 2013;504(7478):138-42.
37. Cerami E, et al. The cBio cancer genomics portal: an open platform for exploring multidimensional cancer genomics data. *Cancer Discov.* 2012;2(5):401-4.
38. Uljon S, et al. Structural Basis for Substrate Selectivity of the E3 Ligase COP1. *Structure.* 2016;24(5):687-96.
39. Lito P, et al. Relief of profound feedback inhibition of mitogenic signaling by RAF inhibitors attenuates their activity in BRAFV600E melanomas. *Cancer Cell.* 2012;22(5):668-82.
40. Wagle N, et al. MAP kinase pathway alterations in BRAF-mutant melanoma patients with acquired resistance to combined RAF/MEK inhibition. *Cancer Discov.* 2014;4(1):61-8.
41. Hugo W, et al. Non-genomic and Immune Evolution of Melanoma Acquiring MAPKi Resistance. *Cell.* 2015;162(6):1271-85.

42. Straussman R, et al. Tumour micro-environment elicits innate resistance to RAF inhibitors through HGF secretion. *Nature.* 2012;487(7408):500-4.
43. Wiesner T, et al. Alternative transcription initiation leads to expression of a novel ALK isoform in cancer. *Nature.* 2015;526(7573):453-7.
44. Wang B, et al. ATXN1L, CIC, and ETS Transcription Factors Modulate Sensitivity to MAPK Pathway Inhibition. *Cell Rep.* 2017;18(6):1543-57.
45. Liao S, Davoli T, Leng Y, Li MZ, Xu Q, and Elledge SJ. A genetic interaction analysis identifies cancer drivers that modify EGFR dependency. *Genes Dev.* 2017;31(2):184-96.

Figure Legends

Figure 1. ETV1 is a downstream transcriptional effector of MAPK signaling. GSEA enrichment plots of ETV1sh2-downregulated gene set on gene expression profiles of MAPK pathway inhibition by PD325901 (PD901) in GIST48 and GIST882 cells, imatinib (Imat) in GIST-T1 cells and vemurafenib (Vemu) in A375 and Colo800 cells.

Figure 2. ETV1 modulates MAPK homeostasis through regulation of MAPK negative-feedback regulators. (**A**) Heatmap of genome-wide ETV1 ChIP-seq signals from -1kb to +1kb around ETV1 binding sites in GIST and melanoma cells of promoters and enhancers. Unsupervised k-means clustering of enhancer peaks cluster peaks into shared, melanoma-specific and GIST-specific ETV1 binding sites. (**B**) Venn diagrams showing common genes bound by ETV1 and downregulated by MAPK pathway inhibition in all GIST (top) and melanoma (bottom) cell lines. The shared ETV1-bound and MAPK-regulated genes by both GIST and melanoma lineages are listed. (**C**) ETV1 ChIP-seq signals at the DUSP6, SPRY4, SPRED1 and SPRED2 genomic loci in GIST and melanoma cells. (**D**) Immunoblots of the indicated proteins in GIST882 and A375 cells transfected with scrambled control siRNA (siSCR), siRNAs against ETV1 (siETV1), ETV4 (siETV4) and ETV5 (siETV5).

Figure 3. Genome-wide RNAi screen identifies key regulators of MAPK signaling-dependent ETV1 protein stability. (**A**) A schematic of the MAPK-ETV1 protein stability sensor construct with EGFP-ETV1 fusion protein and tdTomato expressed under the same promoter. (**B**) Immunoblots of EGFP and GAPDH in A2058 melanoma cells expressing EGFP or EGFP fused to full-length ETV1 (EGFP-flETV1), or the amino terminal 174 amino-acids of

ETV1 (EGFP-nETV1) and treated with DMSO (Veh), 1 μM vemurafenib (Vemu), or MG132 for 8 hours. (**C**) FACS plot of tdTomato and EGFP fluorescence in A2058 cells expressing EGFP-nETV1-IRES-tdTomato treated with DMSO (Veh) or 1μM vemurafenib (Vemu) for 24 hours. (**D**) Histogram of EGFP/tdTomato fluorescence ratio in EGFP-nETV1-IRES-tdTomato expressing A2058 cells transduced with shRNA-mir against scrambled (shScr) or BRAF (shBRAF) and treated with DMSO (Veh) or 1μM vemurafenib (Vemu). (**E**) Schematic flow of screen. EGFP-nETV1-IRES-tdTomato-expressing A2058 cells were transduced with a genome-wide shRNA library. Cells were treated with vemurafenib for 24 hours prior to each sort. (**F**) A schematic of the role of selected hits in MAPK signaling-dependent regulation of ETV1 protein degradation. (**G**) Histogram of mCherry fluorescence of A375 cells expressing mCherry-nETV1 sensor treated with DMSO (Veh) or 1μM vemurafenib (Vemu) for 20 hours. (**H**) FACS plots of turboGFP (tGFP) fluorescence linked to shRNA expression and mCherry-nETV1 fluorescence. A375 cells expressing mCherry-nETV1 and indicated shRNA transduced at ~MOI=0.5 and treated with 1μM vemurafenib (Vemu) or DMSO (Veh) for additional 24 hours.

Figure 4. COP1 couples MAPK signaling through MAPK-dependent regulation of ETV1 protein stability. (**A**) Immunoblots of the indicated proteins in GIST882 cells transfected with control (siSCR) or COP1-specific (siCOP1) siRNAs for 48 hours, followed by treatment with vehicle (Veh), imatinib (IM) (1μM) or PD325901 (PD901, 100 nM) for 0.5 or 2 hrs. (**B**) Immunoblot of indicated proteins in A375 cells transfected with control (siSCR) or COP1-specific siRNA (siCOP1) for 48 hrs, followed by treatment with vehicle (Veh), or vemurafenib (Vemu, 1 μM) or trametinib (Tram, 100 nM) for 0.5 or 2 hrs.

Figure 5. COP1 couples MAPK downstream transcriptional output through MAPK-dependent regulation of ETV1 protein stability. (A) GIST882 MAPK median Z-score (defined as the normalized median of genes downregulated by >2-fold, 8 hrs after PD325901 (PD901) treatment in GIST882 cells) in GIST882 cells transfected with scrambled siRNA (siSCR) or two siRNAs against COP1, and treated with vehicle (Veh) or PD901 (100 nM) for 8 hrs. n=2, Error bars: mean ± SD. (B) Heatmap of GIST882 MAPK genes (change >2-fold, P<0.05 by PD901) gene expression changes in GIST882 cells under the indicated conditions, from left to right: PD325901 vs. vehicle treatment (PD901Δ), ETV1sh2 vs. shSCR (shETV1Δ), COP1si1 vs. siSCR and with PD325901 treatment (COP1si1Δ in PD901) and COP1si2 vs. siSCR and with PD325901 treatment (COP1si2Δ in PD901). (C) GSEA enrichment plot of a gene set defined by genes upregulated by COP1 knockdown in PD325901 treated GIST882 cells (G882_siCOP1_UP_in_PD901), demonstrating that this gene set is highly negatively enriched among genes downregulated by PD901 compared to vehicle (Veh). (D) A375 MAPK median Z-score in siSCR and siCOP1 transfected A375 cells after treatment with vehicle (Veh), vemurafenib (Vemu, 1 μM) or trametinib (Tram, 100 nM) for 8 hrs. (E) Heatmaps of gene expression changes in A375 cells, from left to right: vemurafenib vs. vehicle treatment in siSCR transfected cells (VemuΔ), shETV1 vs. shSCR (shETV1Δ), vemurafenib treated siCOP1 vs. siSCR transfected cells (siCOP1Δ in Vemu), trametinib treated siCOP1 vs. siSCR transfected cells (siCOP1Δ in Tram). (F) GSEA showing that a gene set defined by genes upregulated by siCOP1 in vemurafenib treated A375 cells is highly negatively enriched among genes downregulated by vemurafenib in A375 cells.

Figure 6. COP1 loss mediates resistance to MAPK pathway inhibition in GIST and melanoma *in vitro*. (**A**) Schematics of CRISPR/Cas9 constructs used in the competition growth assay in GIST-T1. (**B**) Competition growth assays of mixed population of parental GIST-T1 and GIST-T1 cells expressing both a CRISPR/Cas9 vector with either empty (sgCON) or COP1-specific (sgCOP1) sgRNA guide in an EGFP containing vector, under the treatment conditions as indicated, vehicle (Veh), imatinib (IM, 100 nM), or trametinib (Tram, 100 nM). n=3, Error bars: mean ± SD. (**C**) Dose response curves of GIST-T1 cells transduced with CRISPR/Cas9-mediated COP1 knockout (sgCOP1) or a control (sgGFP) and treated with imatinib or trametinib as indicated for 5 days. Cell viability was determined by CellTiter-Glo. n=3, Error bars: mean ± SD. (**D**) Competition growth assay between infected (tGFP-positive) and uninfected (tGFP-negative) A375 cells transduced with shRNA-mir vector targeting scrambled (shSCR) or two COP1 sequences (shCOP1-1, shCOP1-2). The cells were transduced with MOI ~10-30% and were treated 3 days after transduction with vehicle (Veh), vemurafenib (Vemu 100 nM), or trametinib (Tram 5 nM). TurboGFP (tGFP) fluorescence was quantified over time. n=3, Error bars: mean ± SD. (**E**) Dose response curves of A375 cells transduced with CRISPR/Cas9-mediated COP1 knockout (sgCOP1) or a control (sgGFP) and treated with vemurafenib or trematinib as indicated for 5 days. Cell viability was determined by CellTiter-Glo. n=3, Error bars: mean ± SD.

Figure 7. Stabilized ETV1 protein mediates resistance to MAPK pathway inhibition in melanoma cells. (**A**) Amino acid (aa) sequence of ETV1 (aa59-aa74) containing two adjacent COP1 binding motifs (ExxVPD) and of mutation of both VPD motifs to AAD. (**B**) Immunoblot of indicated proteins from ETV1-immunoprecipitants (IP) from 293T cells expressing vector

control containing EGFP (vector), $ETV1^{WT}$ or $ETV1^{AAD}$ mutant proteins. (**C**) Immunoblot of ETV1 and GAPDH in A375 cells expressing vector control (EGFP), $ETV1^{WT}$ or $ETV1^{AAD}$ proteins, and treated with vehicle (Veh), vemurafenib (Vemu, 1μM) or trametinib (Tram, 100nM) for 8 hours. (**D**) Dose response curves of A375 cells expressing control (EGFP), $ETV1^{WT}$ or $ETV1^{AAD}$ proteins, and treated with vemurafenib or trametinib for 5 days. n=3, Error bars: mean ± SD. (**E**) Growth competition assay between parental and A375 cells transduced with an IRES-EGFP vector expressing control EGFP, $ETV1^{WT}$ or $ETV1^{AAD}$ proteins and treated with vehicle (Veh), vemurafenib (Vemu, 100 nM) or trametinib (Tram, 5 nM) over time as indicated. n=3, Error bars: mean ± SD.

Figure 8. COP1 loss mediates resistance to MAPK pathway inhibitors in vivo. (**A-B**) Immunoblots of two representative GIST-T1 (**A**) or A375 (**B**) xenografted tumors with (sgCOP1) or without COP1 knockout (sgGFP) explanted 2 days after drug treatment by oral gavage of agents as indicated. Vehicle (Veh): water; imatinib (IM): 80 mg/kg twice daily; vemurafenib (Vemu): 100 mg/kg twice daily. sgGFP: control guide; sgCOP1: single guide targeting COP1. (**C-D**) Growth curves of GIST-T1 (**C**) or A375 (**D**) xenografts in SCID mice over time with treatment as indicated by oral gavage. Vehicle: water; imatinib: 80 mg/kg twice daily; vemurafenib: 75 mg/kg for day 1-day 7, and increased to 100 mg/kg for day 8-day14, twice daily. GIST-T1 xenografts: sgGFP vehicle (n=8), sgGFP imatinib (n=18), sgCOP1 vehicle (n=8), sgCOP1 imatinib (n=18); A375 xenografts: sgGFP vehicle (n=10), sgGFP vemurafenib (n=12), sgCOP1 vehicle (n=8), sgCOP1 vemurafenib (n=12). Error bars: mean ± SEM. Two-tailed unpaired t test: **, P=0.0043; ***, P =0.0002; ****, $P < 0.0001$.

Figure 9. Functional characterization of cancer derived COP1 mutations. (**A**) FACS plot of mCherry fluorescence in A375 cells expressing mCherry-nETV1 and indicated sgCOP1 guide RNA or sgCON control (lentiCRISPRv2 vector with no guide RNA). (**B**) FACS plot of mCherry fluorescence in A375 cells expressing mCherry-nETV1 and indicated sgCOP1 guide RNA or sgCON control treated with DMSO (Veh) or 1μM vemurafenib (Vemu) for 24 hours. (**C**) Immunoblot of HA in A375 melanoma cells expressing wild-type and mutant HA-COP1. Mutations that showed decreased function are in red. (**D**) FACS plots of EGFP and mCherry fluorescence in A375 cells expressing mCherry-nETV1 and either EGFP only or with the indicated COP1 mutation treated with 1μM vemurafenib (Vemu) or DMSO (Veh) for 24 hours. (**E**) Model of structure of COP1 WD40 Domain together with peptide ((DEQFVPDY). The protein backbone is shown as cartoons and the surface is in white, with key interface side chains labeled and rendered as sticks. The ETV1 peptide backbone is shown in green with nitrogen atom in blue and oxygen atom in red. Functional COP mutant amino acids are labeled in black and loss of function mutant amino acids are in red.

Figure10. Functional characterization of *de novo* DET1 mutations in vemurafenib treated melanoma patients. (**A**) Immunoblot of indicated proteins in A375 cells expressing CRISPR/Cas9 with guide against DET1 (sgDET1) or vector control with no guide (sgCON), and treated with vehicle (Veh), vemurafenib (Vemu, 1 μM) or trametinib (Tram, 100 nM) for 0.5 or 2 hours. (**B**) FACS plot of mCherry fluorescence in A375 cells expressing mCherry-nETV1 and indicated sgCON or sgDET1 guide RNAs. (**C**) FACS plot of mCherry fluorescence in A375 cells expressing mCherry-nETV1 and indicated sgCON or sgDET1 guide RNAs treated with DMSO (Veh) or 1μM vemurafenib (Vemu) for 24 hours. (**D**) FACS plots of EGFP and mCherry

fluorescence in A375 cells expressing mCherry-nETV1 and either EGFP only or with the indicated DET1 mutation treated with 1μM vemurafenib (Vemu) or DMSO (Veh) for 24 hours. (**E**) HA immunoblots of HA-tagged DET1 in A375 melanoma cells expressing EGFP alone or with DET1 mutations.

Tables

Table 1. The normalized enrichment score (NES) and false discovery rate (FDR) q-value of hETV1-downregulated gene set in each cell line are shown in tables.

	Gene Set	NES	FDR q
GIST48	GIST48_ETV1sh1_DN	-2.38	0.000
	GIST48_ETV1sh2_DN	-2.29	0.000
	GIST-T1_ETV1sh1_DN	-2.15	0.002
	GIST882_ETV1sh2_DN	-2.07	0.004
	GIST882_ETV1sh1_DN	-1.90	0.030
	GIST-T1_ETV1sh2_DN	-1.89	0.032
	COLO800_ETV1sh1_DN	-1.44	0.059
	A375_ETV1sh2_DN	-1.41	0.066
	COLO800_ETV1sh2_DN	-1.40	0.067
	A375_ETV1sh1_DN	NA	NA
GIST882	GIST882_ETV1sh2_DN	-2.37	0.000
	GIST882_ETV1sh1_DN	-2.30	0.000
	GIST48_ETV1sh1_DN	-2.16	0.003
	GIST48_ETV1sh2_DN	-2.12	0.004
	GIST-T1_ETV1sh2_DN	-1.58	0.035
	COLO800_ETV1sh1_DN	-1.43	0.068
	COLO800_ETV1sh2_DN	-1.34	0.111
	GIST-T1_ETV1sh1_DN	-1.28	0.134
	A375_ETV1sh2_DN	NA	NA
	A375_ETV1sh1_DN	NA	NA
GIST-T1	GIST-T1_ETV1sh2_DN	-2.97	0.000
	GIST-T1_ETV1sh1_DN	-2.78	0.000
	GIST882_ETV1sh2_DN	-2.41	0.000
	GIST48_ETV1sh2_DN	-2.39	0.000
	GIST48_ETV1sh1_DN	-2.15	0.001
	Colo800_ETV1sh2_DN	-1.66	0.054
	COLO800_ETV1sh1_DN	-1.46	0.035
	A375_ETV1sh1_DN	-1.38	0.062
	GIST882_ETV1sh1_DN	-1.29	0.103
	A375_ETV1sh2_DN	NA	NA
A375	A375_ETV1sh2_DN	-2.19	0.000
	GIST48_ETV1sh1_DN	-2.04	0.002
	Colo800_ETV1sh2_DN	-1.88	0.010

	GIST882_ETV1sh2_DN	-1.79	0.021
	Colo800_ETV1sh1_DN	-1.75	0.027
	A375_ETV1sh1_DN	-1.74	0.028
	GIST48_ETV1sh2_DN	-1.67	0.044
	GIST882_ETV1sh1_DN	-1.56	0.028
	GIST-T1_ETV1sh1_DN	-1.42	0.064
	GIST-T1_ETV1sh2_DN	-2.97	0.000
Colo800	A375_ETV1sh2_DN	-2.80	0.000
	Colo800_ETV1sh2_DN	-2.43	0.000
	GIST48_ETV1sh1_DN	-2.26	0.000
	GIST882_ETV1sh2_DN	-2.16	0.000
	GIST-T1_ETV1sh2_DN	-2.03	0.000
	Colo800_ETV1sh1_DN	-1.99	0.000
	GIST48_ETV1sh2_DN	-1.98	0.000
	A375_ETV1sh1_DN	-1.88	0.001
	GIST-T1_ETV1sh1_DN	-1.82	0.002
	GIST882_ETV1sh1_DN	-1.67	0.012

Table 2. Top hits identified by HiTSelect (genes that were ranked in the top 15 in either Sort 2 or Sort 3 AND within the top 1,000 in the other Sort).

Gene	Sort 2 Rank	Sort 3 Rank
COP1 (RFWD2)	4	1
DDB1	1	5
PSMD4	2	7
SR140 (U2SURP)	42	2
UBE3C	3	6
COPS2	8	3
COPS1 (GPS1)	6	4
COPS8	5	223
SFRS11 (SRSF11)	12	8
COPS6	10	160
CCDC55 (NSRP1)	14	310
DET1	819	15

Table 3. Tested COP1 mutations from CBioportol.

Sample name	Cancer Study	AA change	Type
MEL-JWCI-WGS-35	Melanoma (Broad)	N168I	Missense
TCGA-EE-A2GR-06	Melanoma (TCGA)	F205L	Missense
ME048	Melanoma (Broad/DFCI)	E316*	Nonsense
MEL-JWCI-WGS-11	Melanoma (Broad)	R356K	Missense
TCGA-EB-A41B-01	Melanoma (TCGA)	R375S	Missense
TCGA-ER-A19P-06	Melanoma (TCGA)	E464*	Nonsense
YUWAND	Melanoma (Yale)	P526S	Missense
TCGA-EE-A2MS-06	Melanoma (TCGA)	R586C	Missense
TCGA-EE-A185-06	Melanoma (TCGA)	W625S	Missense
TCGA-ER-A42L-06	Melanoma (TCGA)	P630L	Missense
TCGA-GN-A263-01	Melanoma (TCGA)	G658E	Missense
MEL-Ma-Mel-67	Melanoma (Broad)	D690N	Missense
05-123E2_LN	Prostate (FHCRC, 2016)	C159Y	Missense
TCGA-55-8506-01	NSCLC (TCGA 2016)	W517C	Missense
TCGA-55-8506-01	NSCLC (TCGA 2016)	C560R	Missense
TCGA-CG-4442-01	Stomach (TCGA)	N557S	Missense

Table 4. Table of two *de novo* patient derived DET1 mutations arising after vemurafenib treatment.

Sample Name	Cancer Study	AA change	Type
Pat_44_Post	SKCM (BROAD 2014)	A429G	Missense
Pat_41_Post	SKCM (BROAD 2014)	P535F	Missense

Vemurafenib resistant Skin Cutaneous Melanoma (Van Allen et al., 2014)

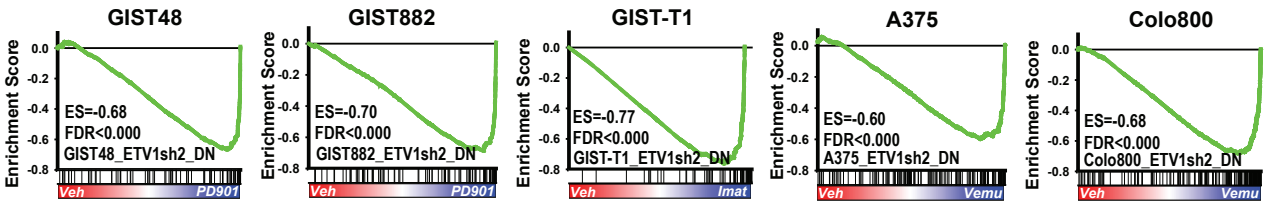

Figure 1. ETV1 is a downstream transcriptional effector of MAPK signaling. GSEA enrichment plots of ETV1sh2-downregulated gene set on gene expression profiles of MAPK pathway inhibition by PD325901 (PD901) in GIST48 and GIST882 cells, imatinib (Imat) in GIST-T1 cells and vemurafenib (Vemu) in A375 and Colo800 cells.

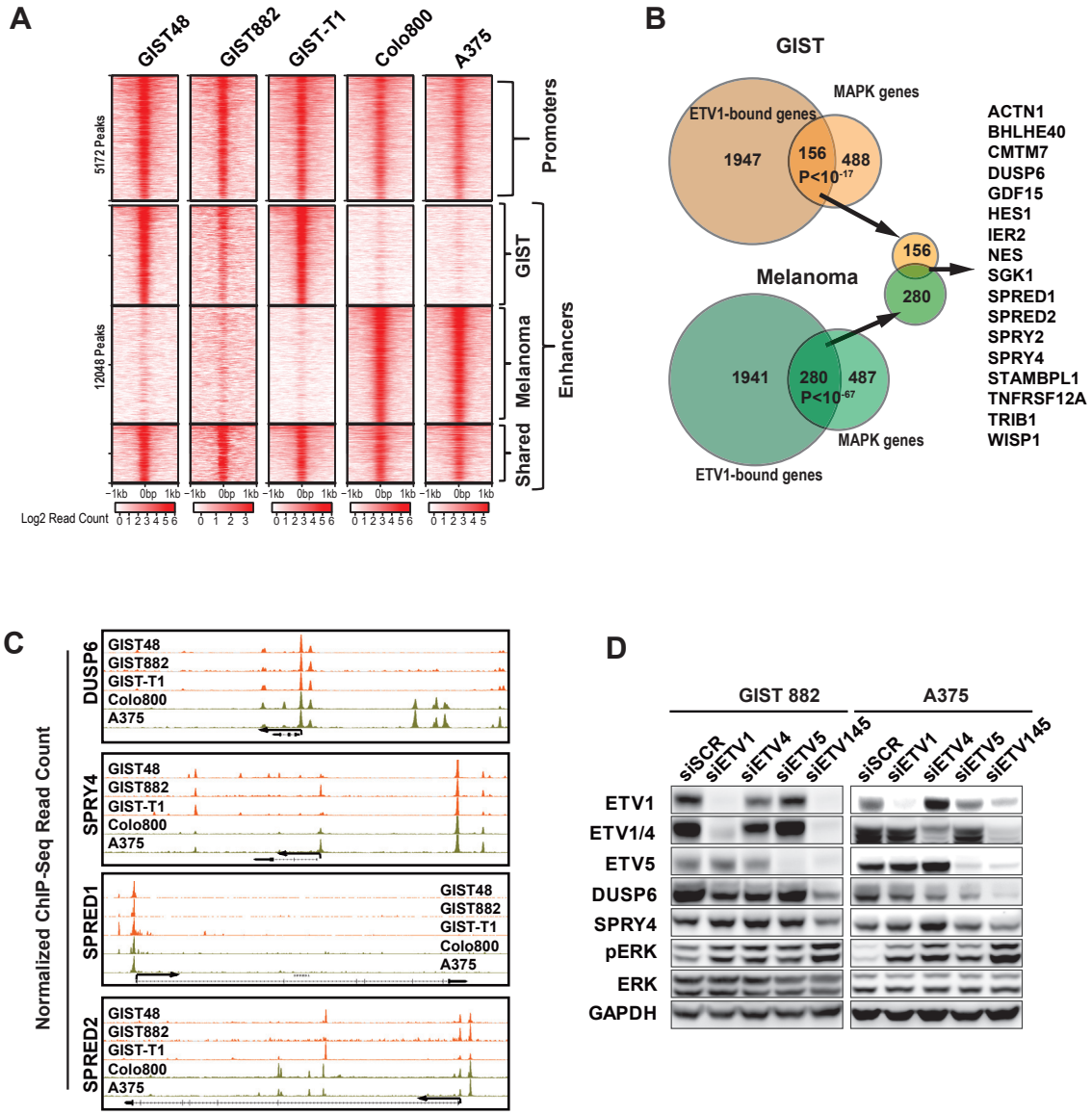

Figure 2. ETV1 modulates MAPK homeostasis through regulation of MAPK negative-feedback regulators. (**A**) Heatmap of genome-wide ETV1 ChIP-seq signals from -1kb to +1kb around ETV1 binding sites in GIST and melanoma cells of promoters and enhancers. Unsupervised k-means clustering of enhancer peaks cluster peaks into shared, melanoma-specific and GIST-specific ETV1 binding sites. (**B**) Venn diagrams showing common genes bound by ETV1 and downregulated by MAPK pathway inhibition in all GIST (top) and melanoma (bottom) cell lines. The shared ETV1-bound and MAPK-regulated genes by both GIST and melanoma lineages are listed. (**C**) ETV1 ChIP-seq signals at the DUSP6, SPRY4, SPRED1 and SPRED2 genomic loci in GIST and melanoma cells. (**D**) Immunoblots of the indicated proteins in GIST882 and A375 cells transfected with scrambled control siRNA (siSCR), siRNAs against ETV1 (siETV1), ETV4 (siETV4), ETV5 (siETV5), or the combination (siETV145) for 48 hours.

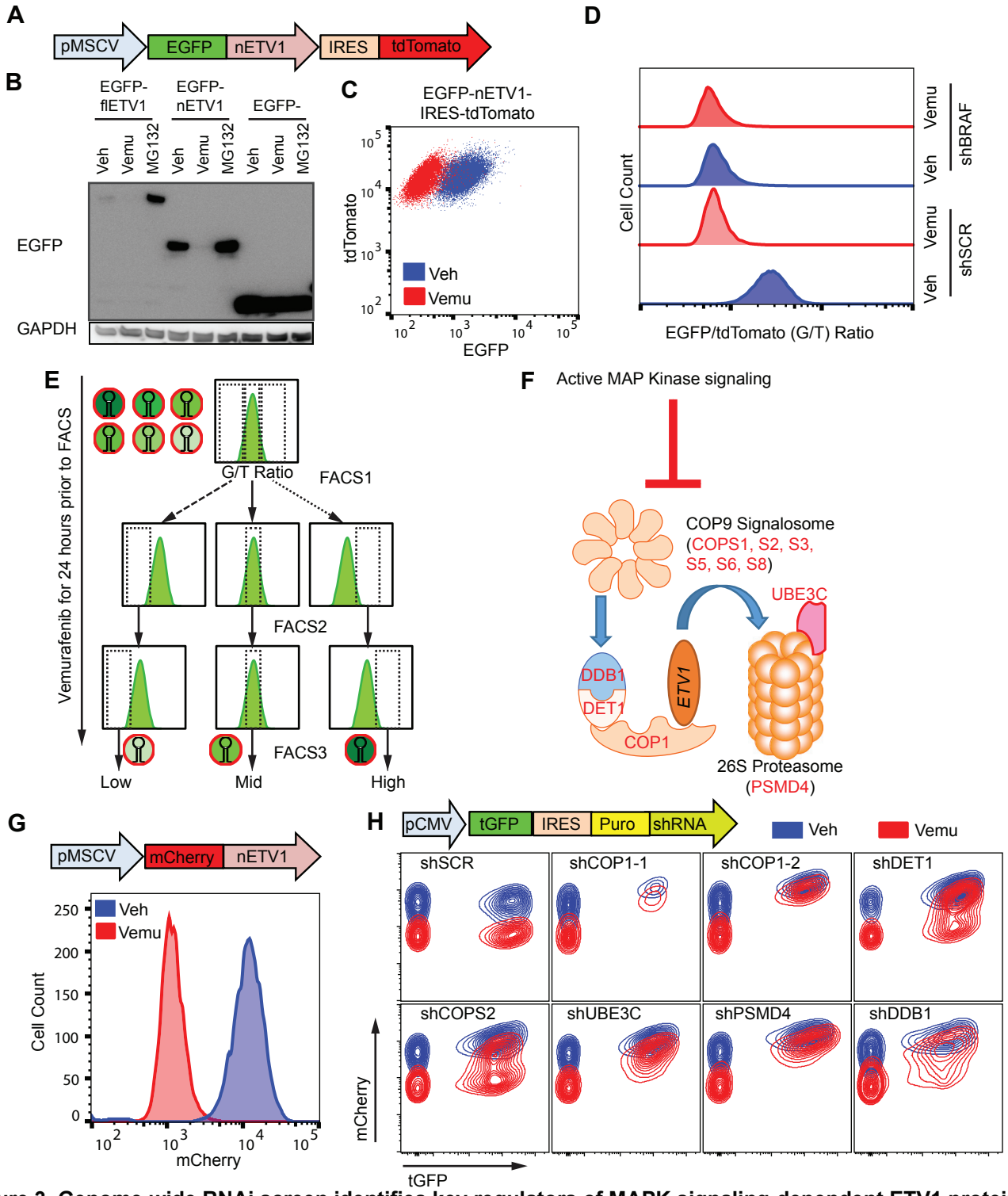

Figure 3. Genome-wide RNAi screen identifies key regulators of MAPK signaling-dependent ETV1 protein stability. (**A**) A schematic of the MAPK-ETV1 protein stability sensor construct with EGFP-ETV1 fusion protein and tdTomato expressed under the same promoter. (**B**) Immunoblots of EGFP and GAPDH in A2058 melanoma cells expressing EGFP or EGFP fused to full-length ETV1 (EGFP-flETV1), or the amino terminal 174 amino-acids of ETV1 (EGFP-nETV1) and treated with DMSO (Veh), 1 μM vemurafenib (Vemu), or MG132 for 8 hours. (**C**) FACS plot of tdTomato and EGFP fluorescence in A2058 cells expressing EGFP-nETV1-IRES-tdTomato treated with DMSO (Veh) or 1μM vemurafenib (Vemu) for 24 hours. (**D**) Histogram of EGFP/tdTomato fluorescence ratio in EGFP-nETV1-IRES-td-Tomato expressing A2058 cells transduced with shRNA-mir against scrambled (shSCR) or BRAF (shBRAF) and treated with DMSO (Veh) or 1μM vemurafenib (Vemu). (**E**) Schematic flow of screen. EGFP-nETV1-IRES-tdTomato-ex-pressing A2058 cells were transduced with a genome-wide shRNA library. Cells were treated with vemurafenib for 24 hours prior to each sort. (**F**) A schematic of the role of selected hits in MAPK signaling-dependent regulation of ETV1 protein degradation. (**G**) Histogram of mCherry fluorescence of A375 cells expressing mCherry-nETV1 sensor treated with DMSO (Veh) or 1μM vemurafenib (Vemu) for 20 hours. (**H**) FACS plots of turboGFP (tGFP) fluorescence linked to shRNA expression and mCherry-nETV1 fluorescence. A375 cells expressing mCherry-nETV1 and indicated shRNA transduced at ~MOI=0.5 and treated with 1μM vemurafenib (Vemu) or DMSO (Veh) for additional 20 hours.

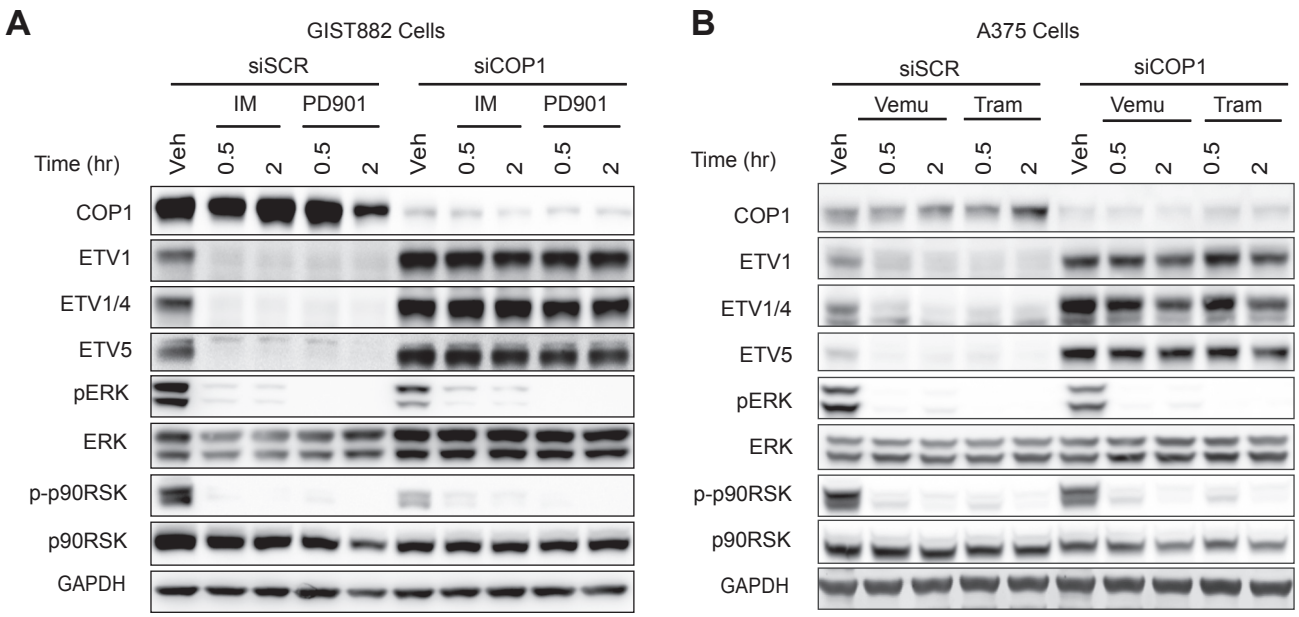

Figure 4. COP1 couples MAPK signaling through MAPK-dependent regulation of ETV1 protein stability. (**A**) Immunoblots of the indicated proteins in GIST882 cells transfected with control (siSCR) or COP1-specific (siCOP1) siRNAs for 48 hours, followed by treatment with vehicle (Veh), imatinib (IM) (1μM) or PD325901 (PD901, 100 nM) for 0.5 or 2 hrs. (**B**) Immunoblot of indicated proteins in A375 cells transfected with control (siSCR) or COP1-specific siRNA (siCOP1) for 48 hrs, followed by treatment with vehicle (Veh), or vemurafenib (Vemu, 1 μM) or trametinib (Tram, 100 nM) for 0.5 or 2 hrs.

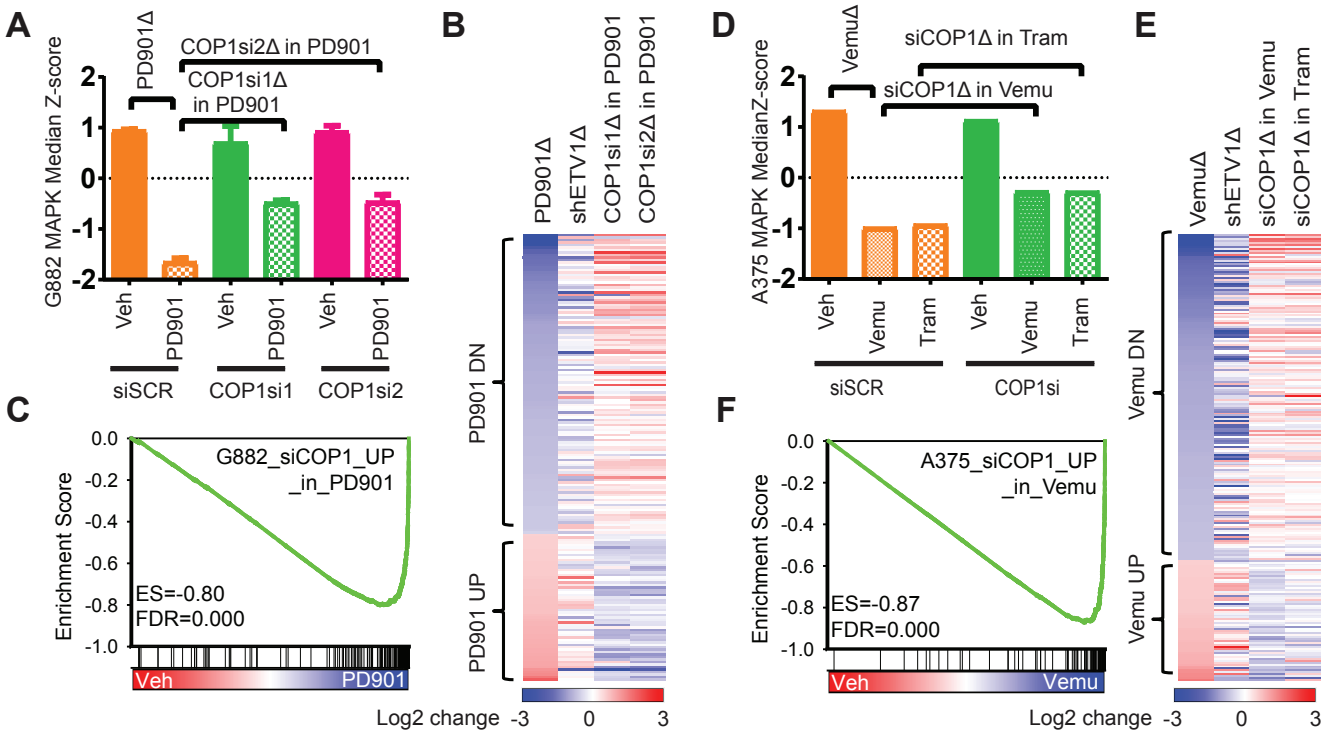

Figure 5. COP1 couples MAPK downstream transcriptional output through MAPK-dependent regulation of ETV1 protein stability. (**A**) GIST882 MAPK median Z-score (defined as the normalized median of genes downregulated by >2-fold, 8 hrs after PD325901 (PD901) treatment in GIST882 cells) in GIST882 cells transfected with scrambled siRNA (siSCR) or two siRNAs against COP1, and treated with vehicle (Veh) or PD901 (100 nM) for 8 hrs. n=2, Error bars: mean ± SD. (**B**) Heatmap of GIST882 MAPK genes (change >2-fold, P<0.05 by PD901) gene expression changes in GIST882 cells under the indicated conditions, from left to right: PD325901 vs. vehicle treatment (PD901Δ), ETV1sh2 vs. shSCR (shETV1Δ), COP1si1 vs. siSCR and with PD325901 treatment (COP1si1Δ in PD901) and COP1si2 vs. siSCR and with PD325901 treatment (COP1si2Δ in PD901). (**C**) GSEA enrichment plot of a gene set defined by genes upregulated by COP1 knock-down in PD325901 treated GIST882 cells (G882_siCOP1_UP_in_PD901), demonstrating that this gene set is highly negatively enriched among genes downregulated by PD901 compared to vehicle (Veh). (**D**) A375 MAPK median Z-score in siSCR and siCOP1 transfected A375 cells after treatment with vehicle (Veh), vemurafenib (Vemu, 1 μM) or trametinib (Tram, 100 nM) for 8 hrs. (**E**) Heatmaps of gene expression changes in A375 cells, from left to right: vemurafenib vs. vehicle treatment in siSCR transfected cells (VemuΔ), shETV1 vs. shSCR (shETV1Δ), vemurafenib treated siCOP1 vs. siSCR transfected cells (siCOP1Δ in Vemu), trametinib treated siCOP1 vs. siSCR transfected cells (siCOP1Δ in Tram). (**F**) GSEA showing that a gene set defined by genes upregulated by siCOP1 in vemurafenib treated A375 cells is highly negatively enriched among genes downregulated by vemurafenib in A375 cells.

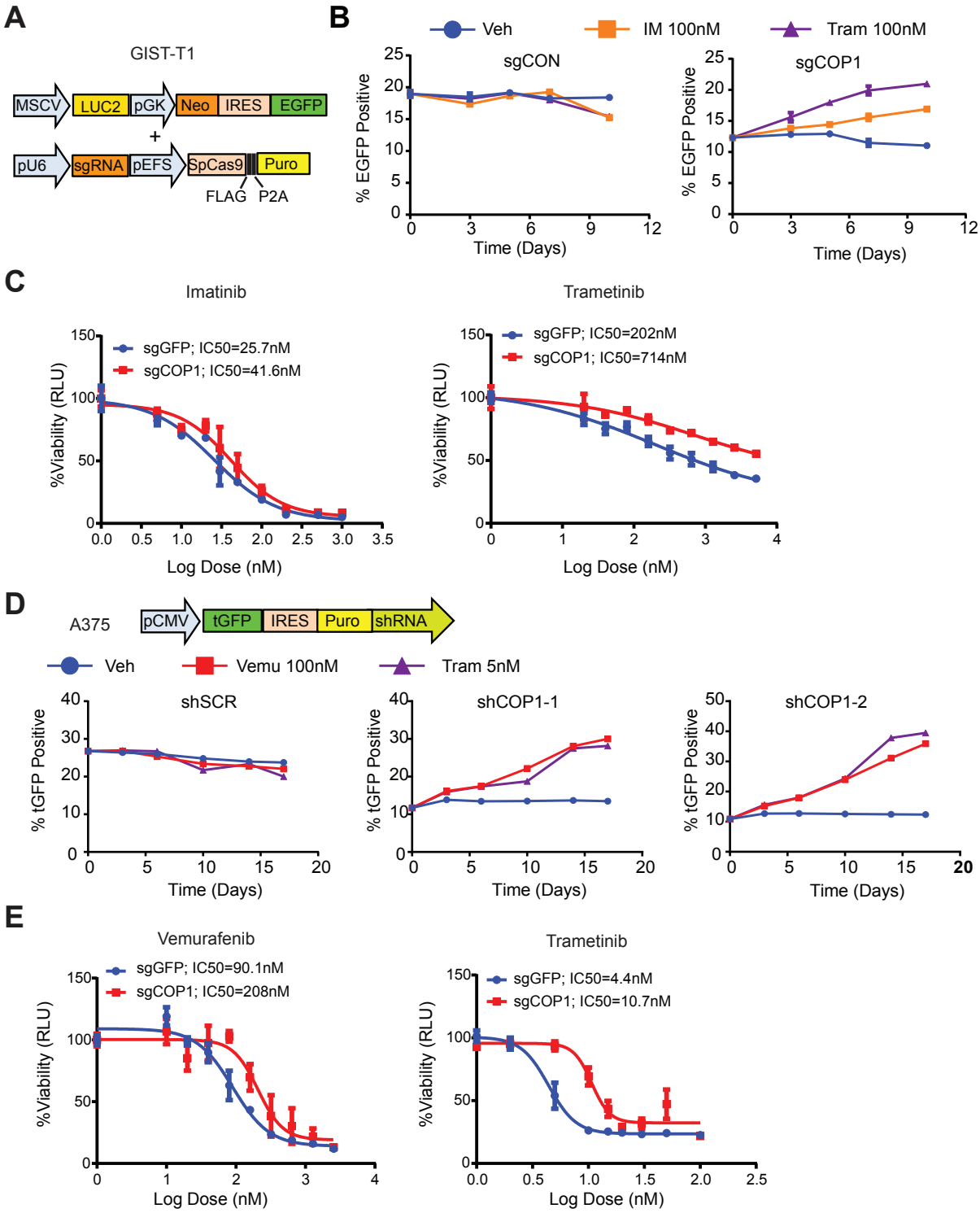

Figure 6. COP1 loss mediates resistance to MAPK pathway inhibition in GIST and melanoma *in vitro*. (**A**) Schematics of CRISPR/Cas9 constructs used in the competition growth assay in GIST-T1. (**B**) Competition growth assays of mixed population of parental GIST-T1 and GIST-T1 cells expressing both a CRISPR/Cas9 vector with either empty (sgCON) or COP1-specific (sgCOP1) sgRNA guide in an EGFP containing vector, under the treatment conditions as indicated, vehicle (Veh), imatinib (IM, 100 nM), or trametinib (Tram, 100 nM). n=3, Error bars: mean ± SD. (**C**) Dose response curves of GIST-T1 cells transduced with CRISPR/Cas9-mediated COP1 knockout (sgCOP1) or a control (sgGFP) and treated with imatinib or trametinib as indicated for 5 days. Cell viability was determined by CellTiter-Glo. n=3, Error bars: mean ± SD. (**D**) Competition growth assay between infected (tGFP-positive) and uninfected (tGFP-negative) A375 cells transduced with shRNA-mir vector targeting scrambled (shSCR) or two COP1 sequences (shCOP1-1, shCOP1-2). The cells were transduced with MOI ~10-30% and were treated 3 days after transduction with vehicle (Veh), vemurafenib (Vemu 100 nM), or trametinib (Tram 5 nM). TurboGFP (tGFP) fluorescence was quantified over time. n=3, Error bars: mean ± SD. (**E**) Dose response curves of A375 cells transduced with CRISPR/Cas9-mediated COP1 knockout (sgCOP1) or a control (sgGFP) and treated with vemurafenib or trematinib as indicated for 5 days. Cell viability was determined by CellTiter-Glo. n=3, Error bars: mean ± SD.

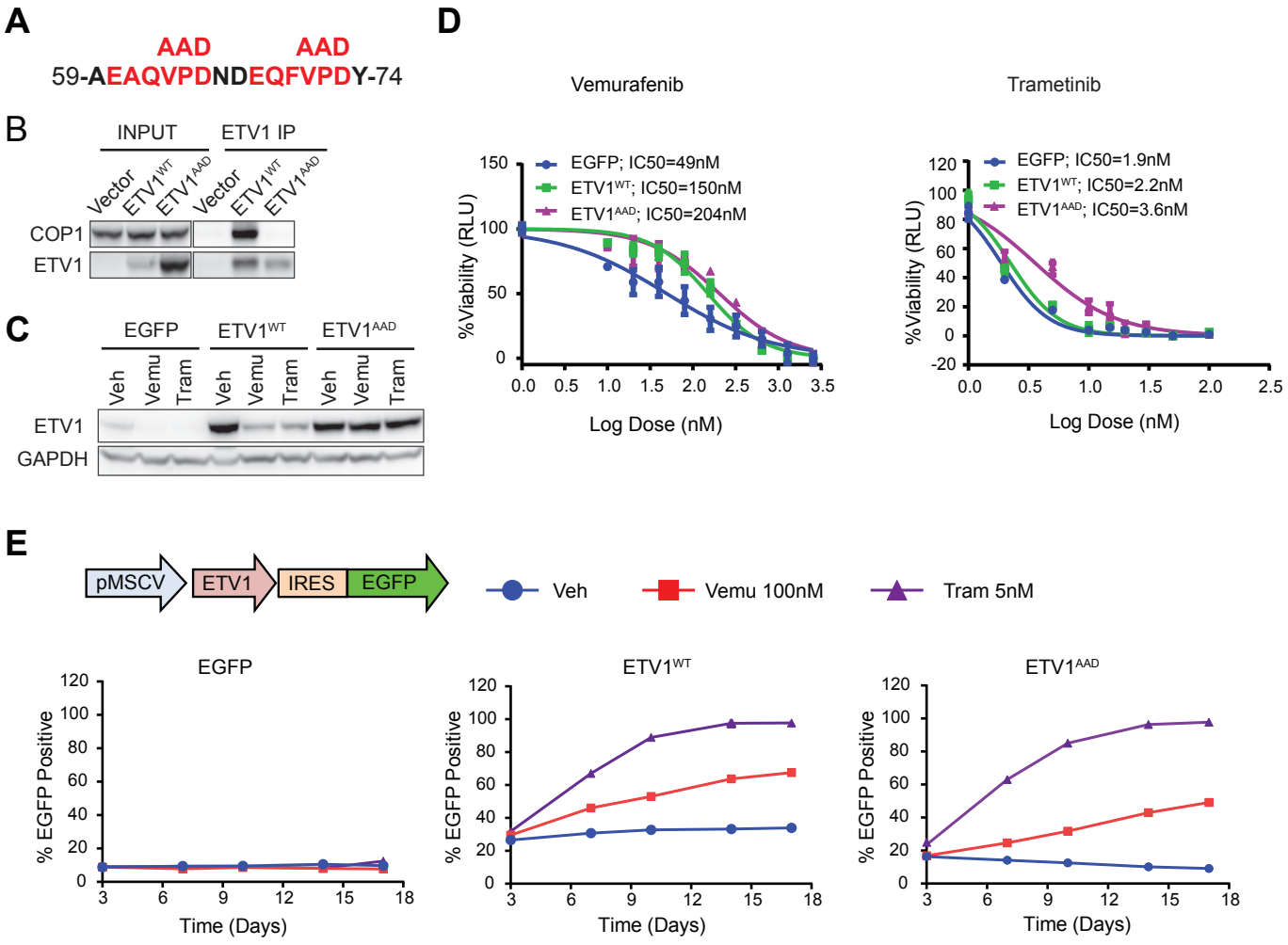

Figure 7. Stabilized ETV1 protein mediates resistance to MAPK pathway inhibition in melanoma cells. (**A**) Amino acid (aa) sequence of ETV1 (aa59-aa74) containing two adjacent COP1 binding motifs (ExxVPD) and of mutation of both VPD motifs to AAD. (**B**) Immunoblot of indicated proteins from ETV1-immunoprecipitants (IP) from 293T cells expressing vector control containing EGFP (vector), ETV1WT or ETV1AAD mutant proteins. (**C**) Immunoblot of ETV1 and GAPDH in A375 cells expressing vector control (EGFP), ETV1WT or ETV1AAD proteins, and treated with vehicle (Veh), vemurafenib (Vemu, 1μM) or trametinib (Tram, 100nM) for 8 hours. (**D**) Dose response curves of A375 cells expressing control (EGFP), ETV1WT or ETV1AAD proteins, and treated with vemurafenib or trametinib for 5 days. n=3, Error bars: mean ± SD. (**E**) Growth competition assay between parental and A375 cells transduced with an IRES-EGFP vector expressing control EGFP, ETV1WT or ETV1AAD proteins and treated with vehicle (Veh), vemurafenib (Vemu, 100 nM) or trametinib (Tram, 5 nM) over time as indicated. n=3, Error bars: mean ± SD.

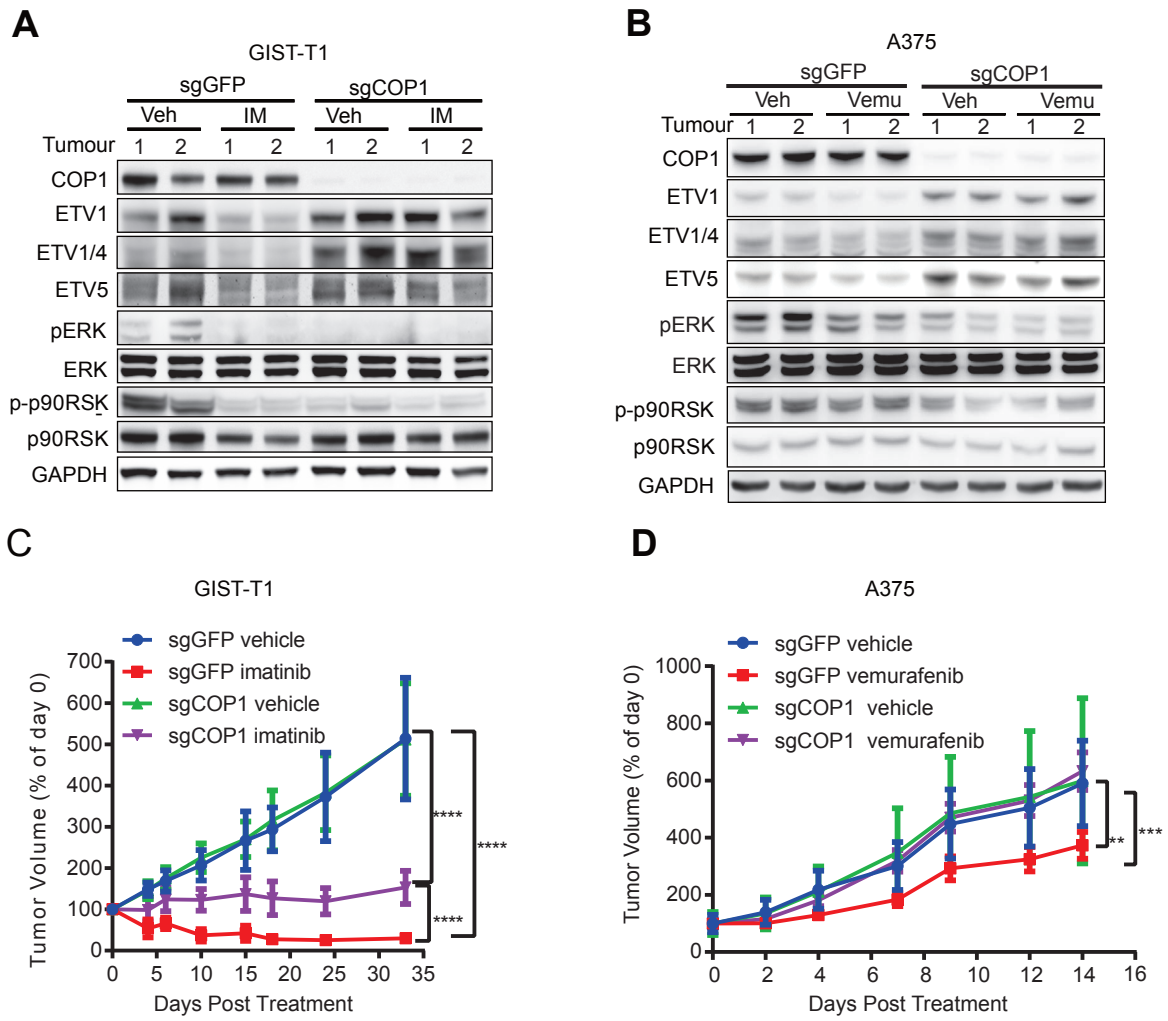

Figure 8. COP1 loss mediates resistance to MAPK pathway inhibitors *in vivo*. (**A**-**B**) Immunoblots of two representative GIST-T1 (**A**) or A375 (**B**) xenografted tumors with (sgCOP1) or without COP1 knockout (sgGFP) explanted 2 days after drug treatment by oral gavage of agents as indicated. Vehicle (Veh): water; imatinib (IM): 80 mg/kg twice daily; vemurafenib (Vemu): 100 mg/kg twice daily. sgGFP: control guide; sgCOP1: single guide targeting COP1. (**C**-**D**) Growth curves of GIST-T1 (**C**) or A375 (**D**) xenografts in SCID mice over time with treatment as indicated by oral gavage. Vehicle: water; imatinib: 80 mg/kg twice daily; vemurafenib: 75 mg/kg for day 1-day 7, and increased to 100 mg/kg for day 8-day14, twice daily. GIST-T1 xenografts: sgGFP vehicle (n=8), sgGFP imatinib (n=18), sgCOP1 vehicle (n=8), sgCOP1 imatinib (n=18); A375 xenografts: sgGFP vehicle (n=10), sgGFP vemurafenib (n=12), sgCOP1 vehicle (n=8), sgCOP1 vemurafenib (n=12). Error bars: mean ± SEM. Two-tailed unpaired t test: **, P=0.0043; ***, P =0.0002; ****, P < 0.0001.

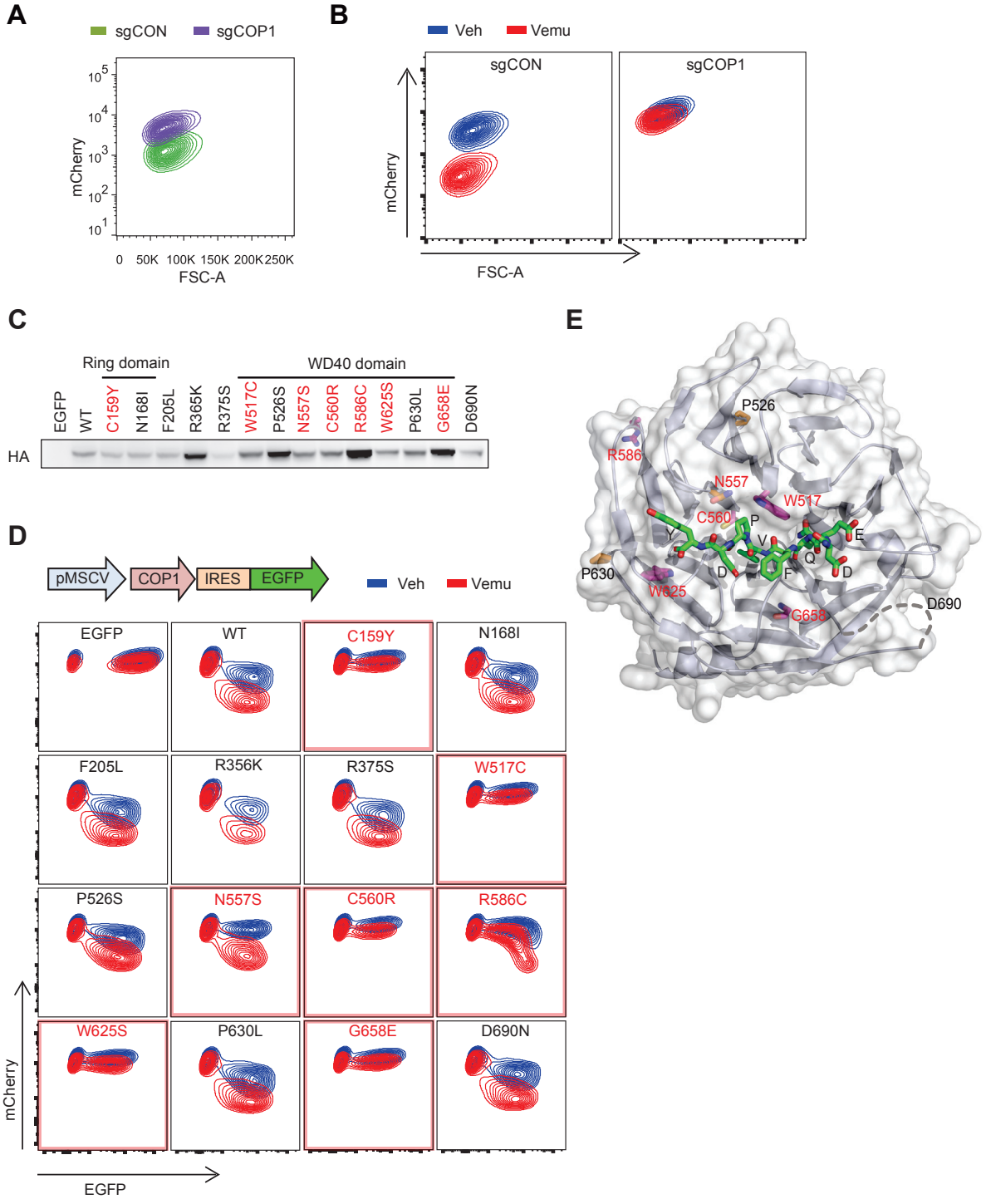

Figure 9. Functional characterization of cancer derived COP1 mutations. (**A**) FACS plot of mCherry fluorescence in A375 cells expressing mCherry-nETV1 and indicated sgCOP1 guide RNA or sgCON control (lentiCRISPRv2 vector with no guide RNA). (**B**) FACS plot of mCherry fluorescence in A375 cells expressing mCherry-nETV1 and indicated sgCOP1 guide RNA or sgCON control treated with DMSO (Veh) or 1μM vemurafenib (Vemu) for 24 hours. (**C**) Immunoblot of HA in A375 melanoma cells expressing wild-type and mutant HA-COP1. Mutations that showed decreased function are in red. (**D**) FACS plots of EGFP and mCherry fluorescence in A375 cells expressing mCherry-nETV1 and either EGFP only or with the indicated COP1 mutation treated with 1μM vemurafenib (Vemu) or DMSO (Veh) for 24 hours. (**E**) Model of structure of COP1 WD40 Domain together with peptide (DEQFVPDY). The protein backbone is shown as cartoons and the surface is in white, with key interface side chains labeled and rendered as sticks. The ETV1 peptide backbone is shown in green with nitrogen atom in blue and oxygen atom in red. Functional COP mutant amino acids are labeled in black and loss of function mutant amino acids are in red.

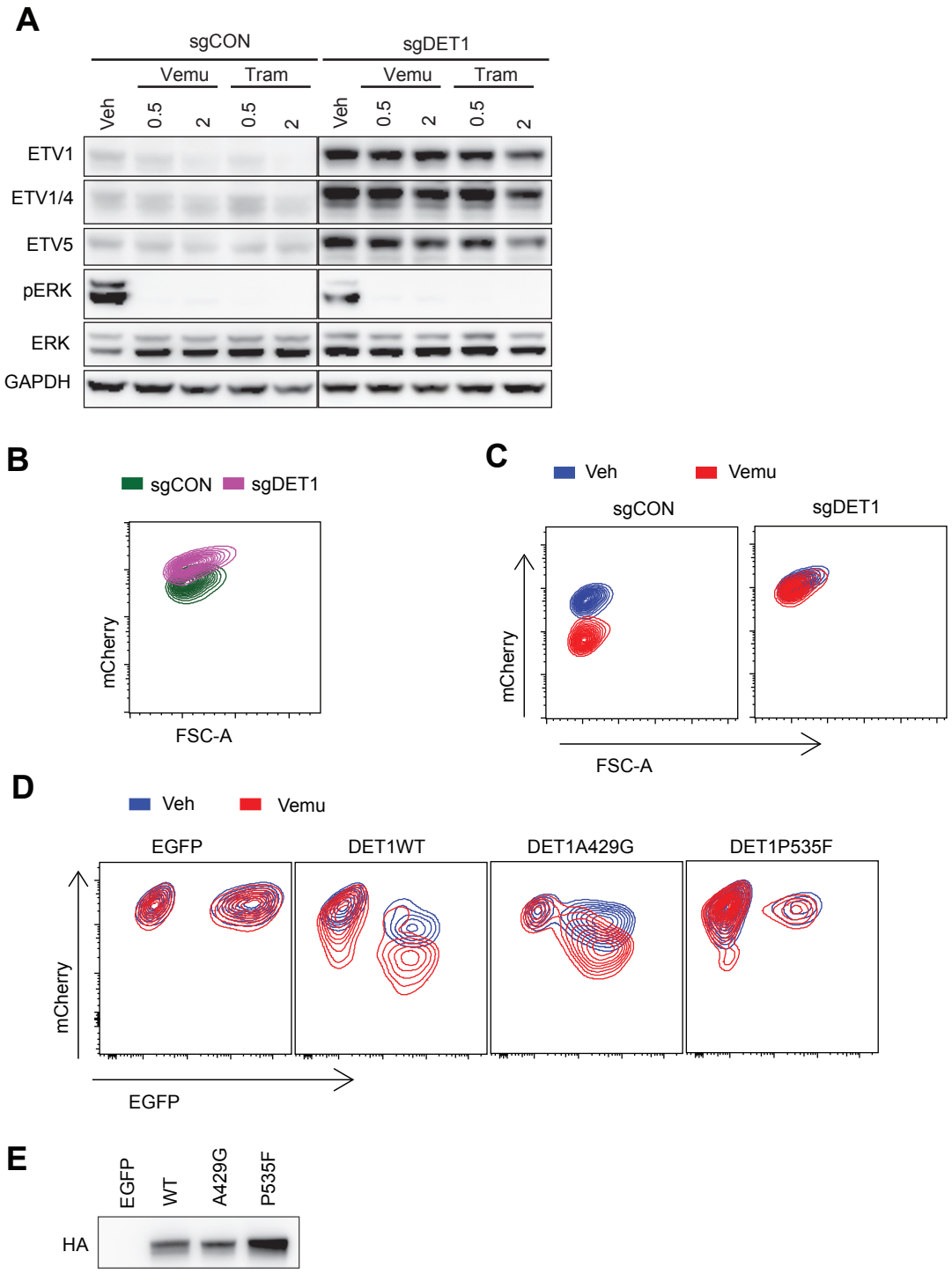

Figure 10. Functional characterization of *de novo* DET1 mutations in vemurafenib treated melanoma patients. (**A**) Immunoblot of indicated proteins in A375 cells expressing CRISPR/Cas9 with guide against DET1 (sgDET1) or vector control with no guide (sgCON), and treated with vehicle (Veh), vemurafenib (Vemu, 1 μM) or trametinib (Tram, 100 nM) for 0.5 or 2 hours. (**B**) FACS plot of mCherry fluorescence in A375 cells expressing mCherry-nETV1 and indicated sgCON or sgDET1 guide RNAs. (**C**) FACS plot of mCherry fluorescence in A375 cells expressing mCherry-nETV1 and indicated sgCON or sgDET1 guide RNAs treated with DMSO (Veh) or 1μM vemurafenib (Vemu) for 24 hours. (**D**) FACS plots of EGFP and mCherry fluorescence in A375 cells expressing mCherry-nETV1 and either EGFP only or with the indicated DET1 mutation treated with 1μM vemurafenib (Vemu) or DMSO (Veh) for 24 hours. (**E**) HA immunoblots of HA-tagged DET1 in A375 melanoma cells expressing EGFP alone or with DET1 mutations.

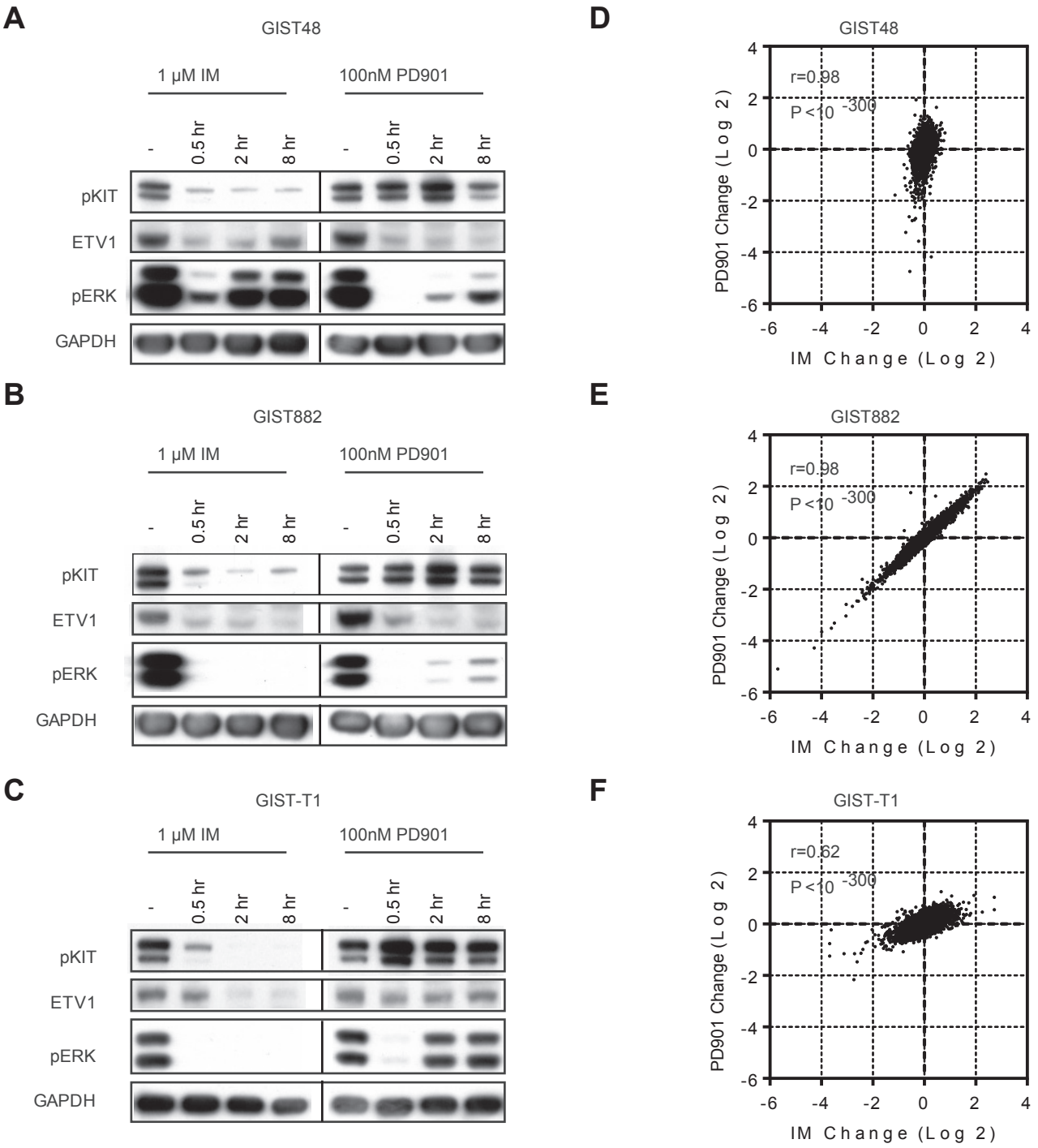

Supplemental Figure 1. Correlation between gene expression changes induced by imatinib and PD325901 in GIST cell lines. (**A**-**C**) Immunoblots of GIST48 (**A**), GIST882 (**B**), and GIST-T1 (**C**) cells treated with vehicle, PD325901 (PD901, 100nM), or imatinib (IM, 1μM) at the indicated time points, demonstrating that imatinib and PD325901 have cell-line specific effects to suppress ERK phosphorylation and ETV1 protein level. (**D**-**F**) Scatter plots of transcriptome changes induced by 8 hours of treatment with PD325901 and imatinib in GIST48 (**D**), GIST882 (**E**) and GIST-T1 (**F**), using Illumina Bead Array microarray (HT-12). R: Correlation coefficient, P: Significance of correlation.

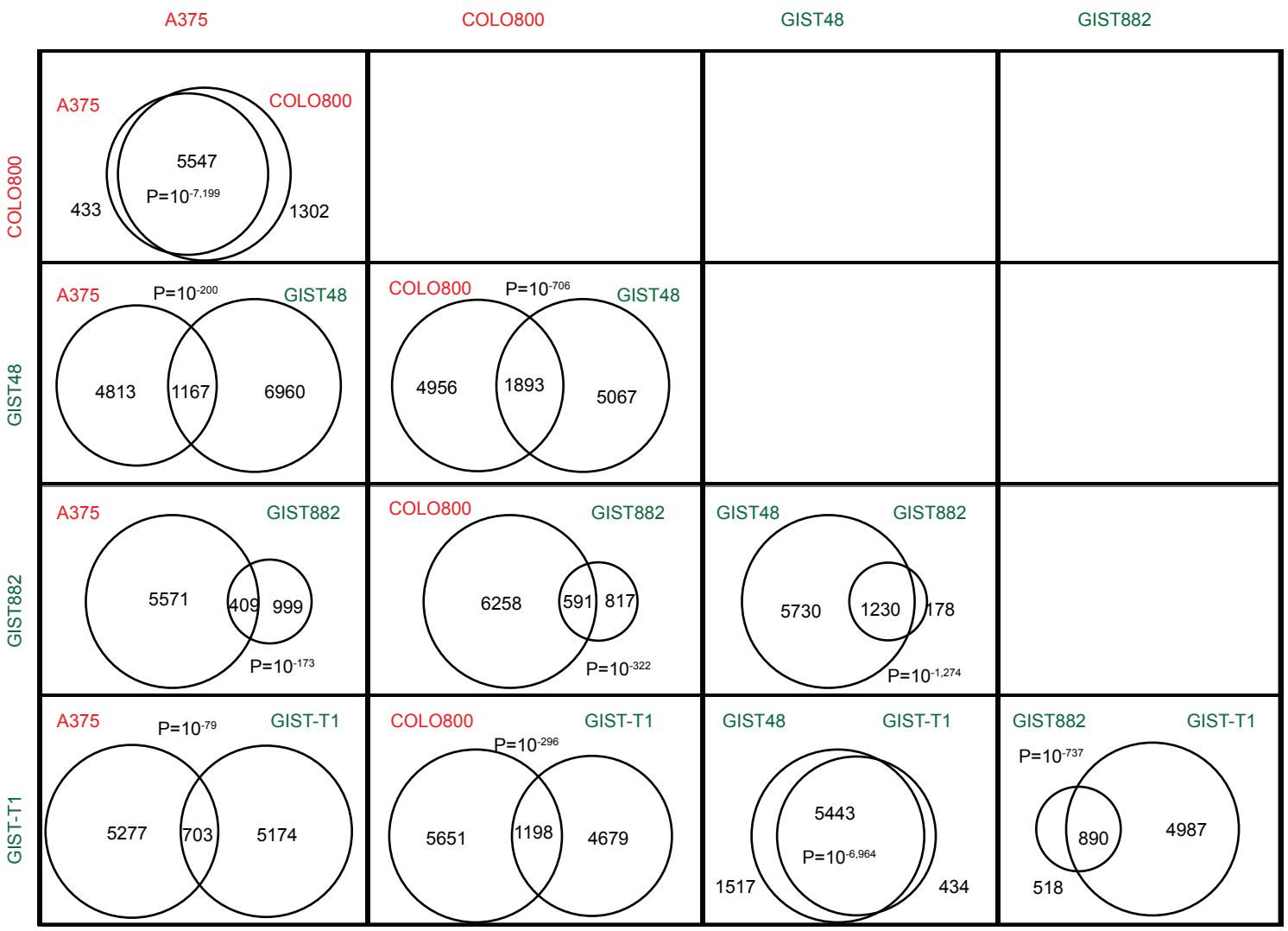

Supplemental Figure 2. Venn diagram of paired comparison of ETV1 enhancer binding sites in GIST and melanoma cell lines. P: Hypergeometric test of overlap assuming the total number of DNA accessible sites is 100,000.

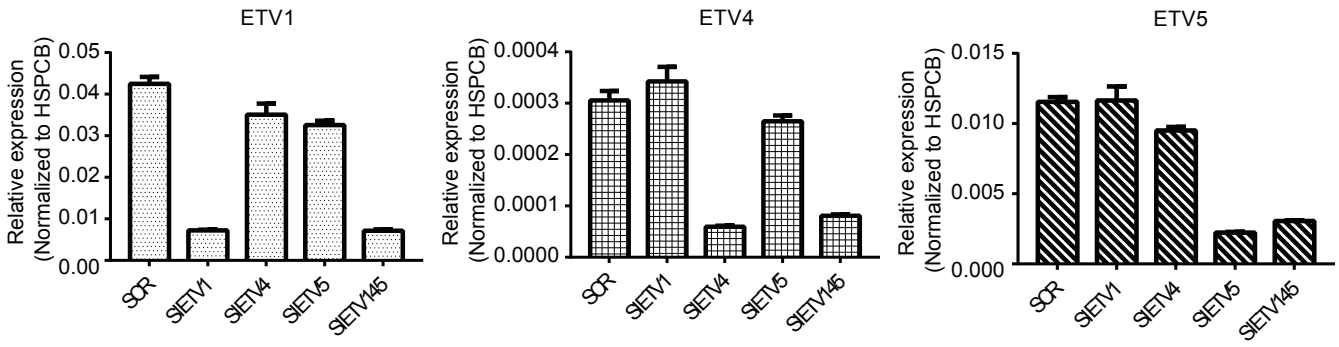

Supplemental Figure 3. Representative qRT-PCR of ETV1, ETV4 and ETV5 after siRNA-mediated knockdown in GIST882 cells. qRT-PCR quantification of ETV1, ETV4, and ETV5 transcripts normalized to the HSPCB housekeeping gene at the indicated knockdown conditions in GIST882 cells 48 hours after transfection.

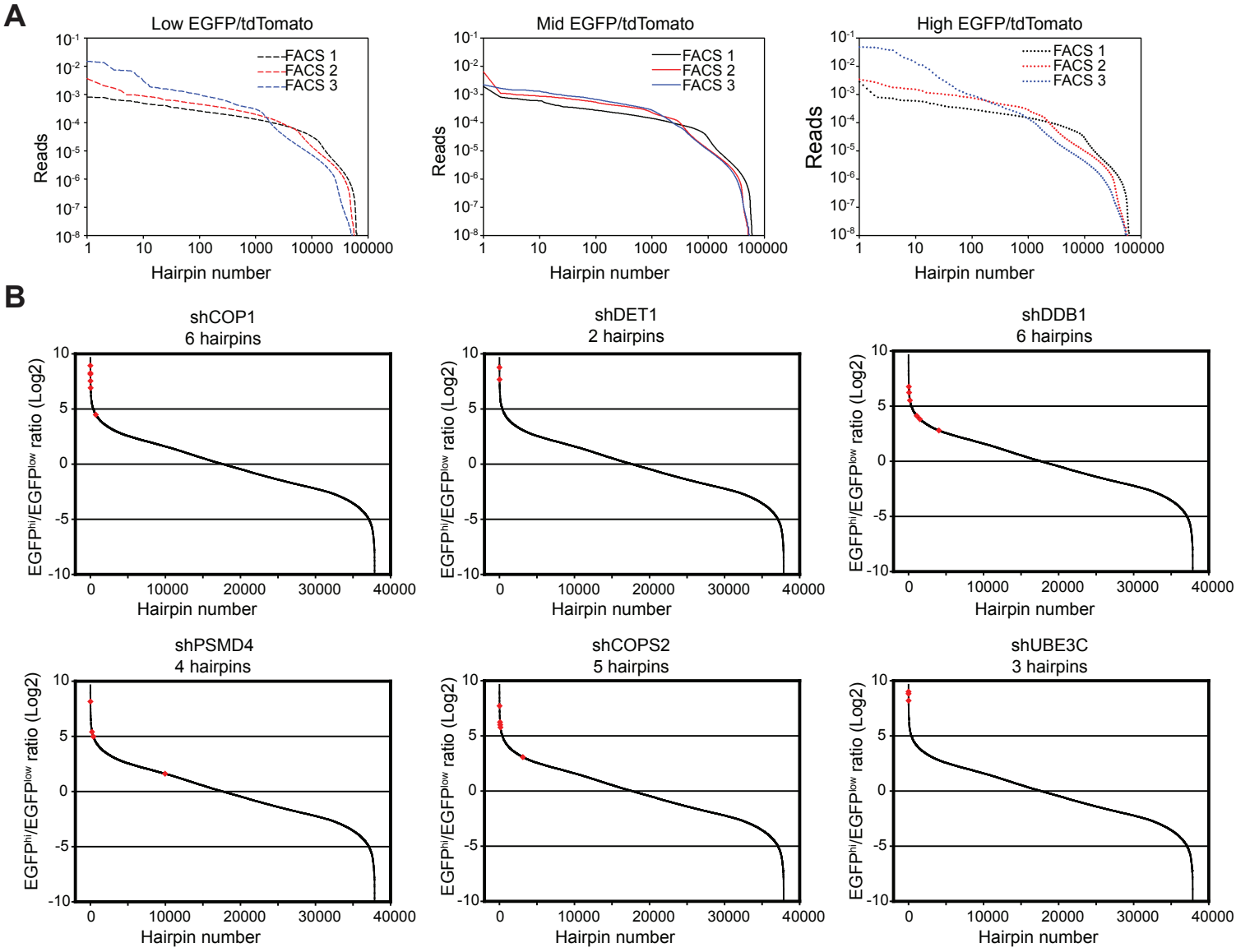

Supplemental Figure 4. Pooled shRNA screen for MAPK signaling-dependent regulators of ETV1 protein stability. (**A**) shRNA hairpin representation of cells FACS sorted for Low, Medium, and High EGFP/tdTomato (E/T) ratio after Sort 1 (FACS 1), Sort 2 (FACS2), and Sort 3 (FACS3). Hairpins are ordered from most to the least number of reads. Y-axis is Log scale of read number. This shows that the hairpin representation shifts over successive sorts for High and Low sorted cells but not for Middle sorted cells, indicating selection of specific hairpins that alter EGFP/tdTomato ratio. (**B**) Hairpins were ranked by ratio of reads between E/T-high to E/T-low population after Sort 3. For specific genes that were highly ranked by HiTSelect (COP1, DET1, DDB1, PSMD4, COPS2, UBE3C), the position of each individual hairpin targeting the gene is shown by red dot.

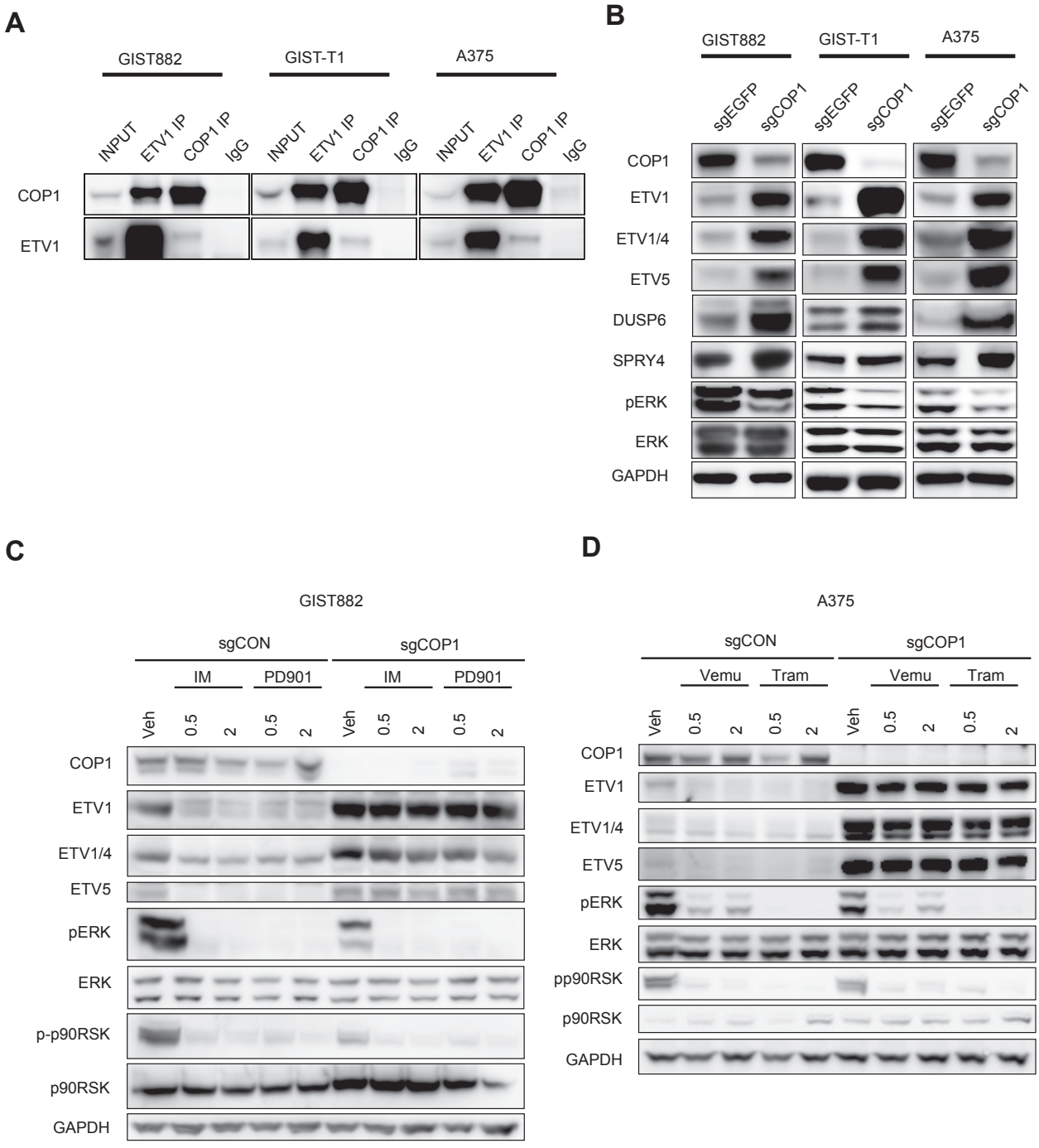

Supplemental Figure 5. Endogenous COP1 and PEA3 ETS interplay in GIST and melanoma cells. (**A**) Immunoblots of COP1 and ETV1 of input lysate, COP1 immunoprecipitant (IP), ETV1 IP, and control rabbit IgG IP from GIST882, GIST-T1, and A375 cells. (**B**) Immunoblots of the indicated proteins in GIST-T1, GIST882 and A375 cells with CRISPR/Cas9-mediated knockout of COP1 (sgCOP1) compared to control (sgEGFP). (**C**) Immunoblots of the indicated proteins in GIST882 cells with CRISPR/Cas9-mediated knockout of COP1 (sgCOP1) or control (sgCON), followed by treatment with vehicle (Veh), imatinib (IM) (1μM) or PD325901 (PD901, 100 nM) for 0.5 or 2 hrs. (**D**) Immunoblot of indicated proteins in A375 cells with CRISPR/Cas9-mediated knockout ofCOP1 (sgCOP1) or control(sgCON), followed by treatment with vehicle (Veh), or vemurafenib (Vemu, 1 μM) or trametinib (Tram, 100 nM) for 0.5 or 2 hrs.

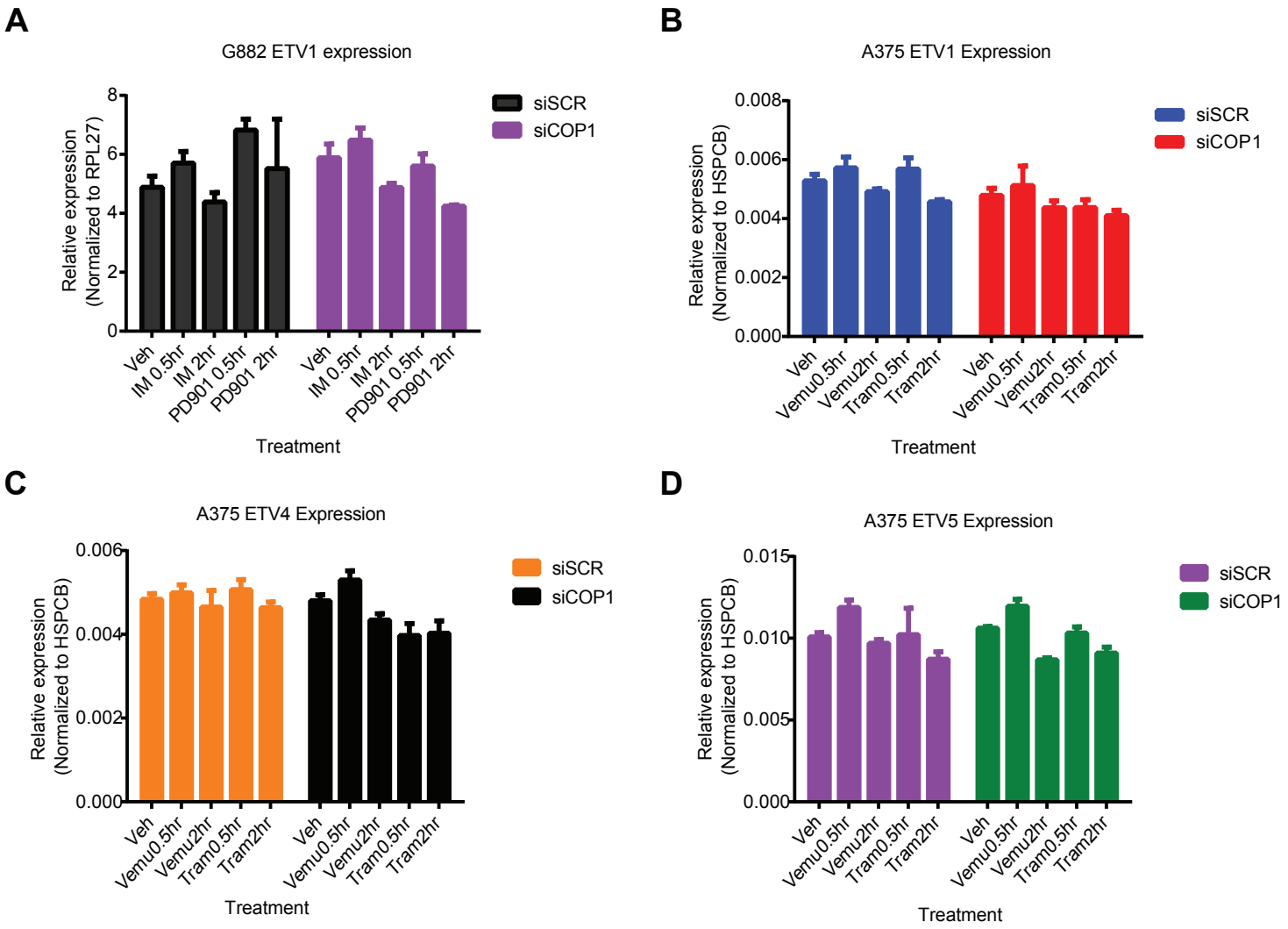

Supplemental Figure 6. Representative qRT-PCR of ETV1, ETV4 and ETV5 after COP1 knockdown and MAPK inhibition. (**A**-**D**) qRT-PCR quantification of ETV1 (**A**-**B**), ETV4 (**C**), and ETV5 (**D**) transcripts at the indicated conditions in GIST882 (**A**) and A375 cells (**B**-**D**). Cells were transfected by siRNA for 48 hours and then treated with drug of 0.5 or 2 hrs. Veh: vehicle; IM: imatinib (1μM); PD901: PD325901 (100 nM); Vemu: vemurafenib (1 μM); Tram: trametinib (100 nM). Error bars: mean ± SD.

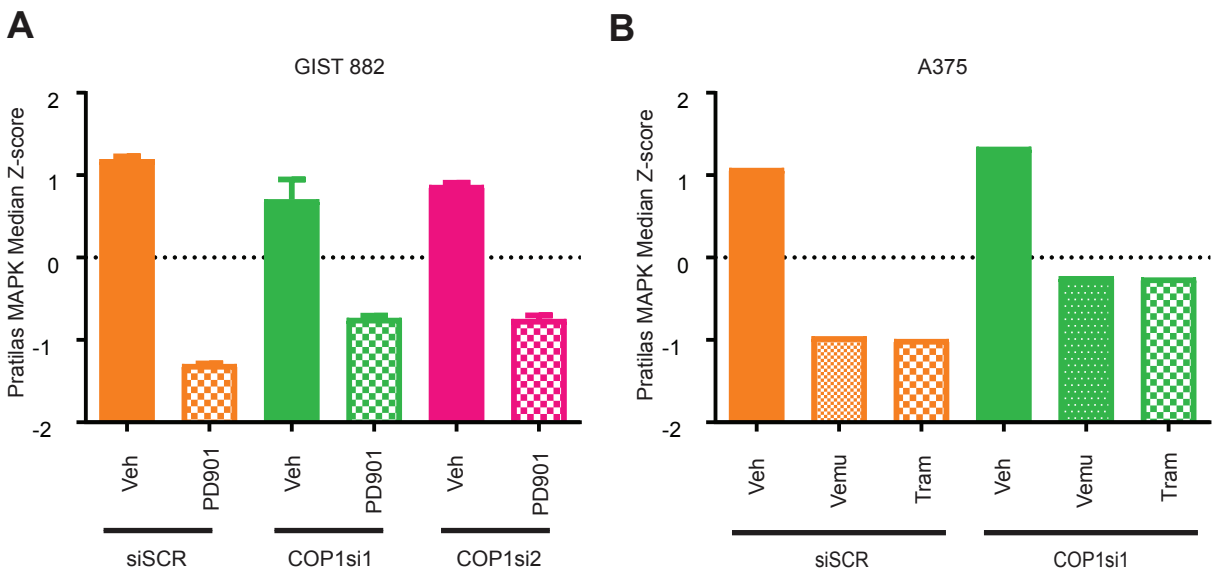

Supplemental Figure 7. Effect of COP1 depletion on consensus MAPK dependent genes. (**A**) Pratilas MAPK median Z-score (15) in GIST882 cells transfected with scrambled siRNA (siSCR) or two siRNAs against COP1, and treated with vehicle (Veh) or PD901 (100 nM) for 8 hrs. n=2, Error bars: mean ± SD. (**B**) Pratilas MAPK median Z-score in A375 cells transfected with scrambled siRNA (siSCR) or COP1si1 and treated with vehicle (Veh), vemurafenib (Vem) or trametinib (Tram) for 8 hrs.

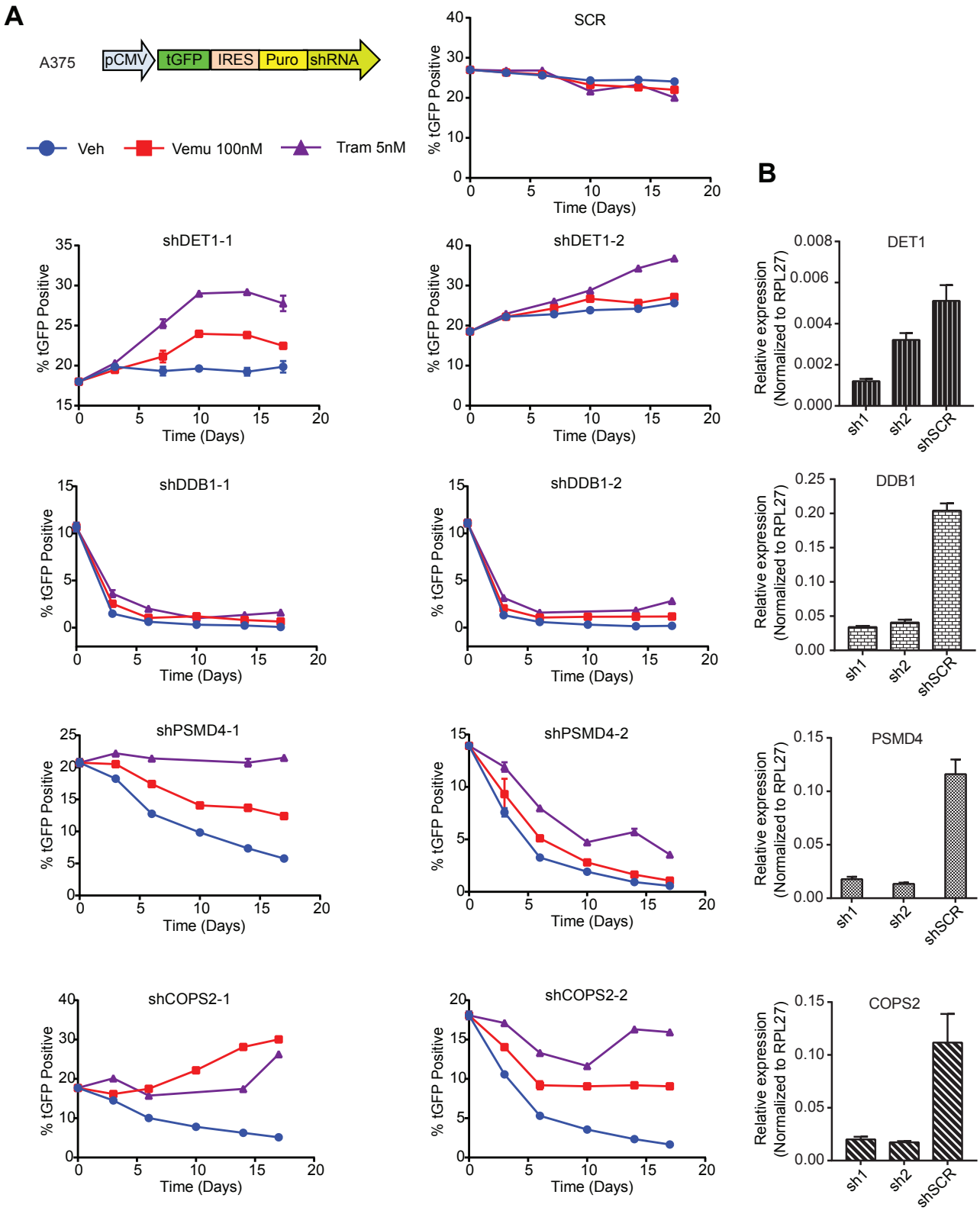

Supplemental Figure 8. Evaluation of other COP1 degradation pathway genes in the regulation of cell growth in response to MAPK pathway inhibition in A375 cells. (**A**) Competition growth assay between infected (tGFP positive) and uninfected (tGFP negative) A375 cells transduced with shRNA-mir vector with scrambled (shSCR) or two independent shRNA specific for DET1, DDB1, PSMD4 or COPS2. The cells were transduced with MOI ~10-30% and were treated 3 days after transduction with vehicle (Veh), vemurafenib (Vemu 100 nM), or trametinib (Tram 5 nM). TurboGFP (tGFP) fluorescence was quantified over time. n=3, Error bars: mean ± SD. (**B**) qRT-PCR quantification of DET1, DDB1, PSMD4 and COPS2 transcripts in A375 cells transduced with shRNA-mir vector with scrambled (shSCR) or two independent shRNA specific for DET1, DDB1, PSMD4 or COPS2. Error bars: mean ± SD.

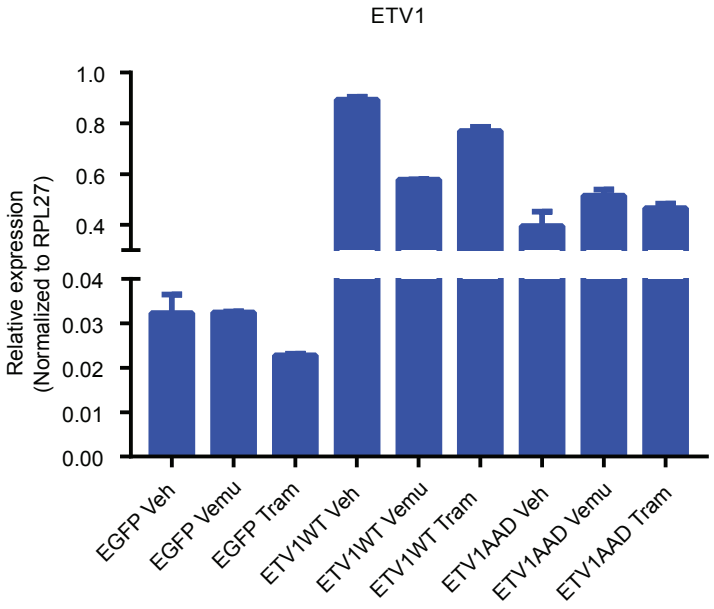

Supplemental Figure 9. Total ETV1 RNA transcript levels of A375 cells expressing exogenous ETV1 under various treatment conditions. qRT-PCR quantification of ETV1 transcripts at the indicated conditions in A375 cells expressing exogenous ETV1WT, ETV1AAD or EGFP control proteins, and treated with vehicle (Veh), vemurafenib (Vemu, 1μM) or trametinib (Tram, 100nM) for 2 hrs. Error bars: mean ± SD.